

SMAI-JCM
SMAI JOURNAL OF
COMPUTATIONAL MATHEMATICS

An all Mach number relaxation
upwind scheme

CHRISTOPHE BERTHON, CHRISTIAN KLINGENBERG & MARKUS ZENK
Volume 6 (2020), p. 1-31.

http://smai-jcm.centre-mersenne.org/item?id=SMAI-JCM_2020__6__1_0

© Société de Mathématiques Appliquées et Industrielles, 2020
Certains droits réservés.

Berthon, Klingenberg, Zenk



Publication membre du
Centre Mersenne pour l'édition scientifique ouverte
<http://www.centre-mersenne.org/>

Sousmission sur <https://smai-jcm.math.cnrs.fr/index.php/SMAI-JCM>





An all Mach number relaxation upwind scheme

CHRISTOPHE BERTHON ¹
CHRISTIAN KLINGENBERG ²
MARKUS ZENK ³

¹ Université de Nantes, CNRS UMR 6629, Laboratoire de Mathématiques Jean Leray, 2 rue de la Houssinière, BP 92208, 44322 Nantes, France.

E-mail address: christophe.berthon@univ-nantes.fr

² Universität Würzburg, Campus Hubland Nord, Emil-Fischer-Strasse 30, 97074 Würzburg, Germany.

E-mail address: klingen@mathematik.uni-wuerzburg.de

³ Universität Würzburg, Campus Hubland Nord, Emil-Fischer-Strasse 30, 97074 Würzburg, Germany.

E-mail address: markus.zenk@gmx.de.

Abstract. The present paper concerns the derivation of finite volume methods to approximate the weak solutions of the Euler equations within all Mach number regimes. To address such an issue, we develop a Suliciu relaxation type scheme. By adopting a relevant scaling according to the Mach number, the obtained numerical scheme is proved to be accurate in the sense that the numerical viscosity does not increase as soon as the Mach number tends to zero. Moreover, the obtained scheme is proved to be asymptotic preserving since the correct incompressible asymptotic regime is recovered in the limit of the Mach number to zero. In addition, the robustness of the method is established since both density and internal energy remain positive during the simulations. Several numerical experiments in 1D and 2D are performed to illustrate the relevance of the proposed low Mach number numerical scheme.

2010 Mathematics Subject Classification. 65M60, 65M12.

Keywords. Hyperbolic system; Euler flow; Low Mach number flows; asymptotic preserving schemes; relaxation schemes; upwind schemes.

1. Introduction

In this work, we consider the approximation of the solutions of the compressible Euler equations of gas dynamics in 2 space dimensions. The system under consideration is given by

$$\begin{cases} \rho_t + (\rho u)_x + (\rho v)_y = 0, \\ (\rho u)_t + (\rho u^2 + p)_x + (\rho uv)_y = 0, \\ (\rho v)_t + (\rho vu)_x + (\rho v^2 + p)_y = 0, \\ E_t + (u(E + p))_x + (v(E + p))_y = 0, \end{cases} \quad (1.1)$$

where $\rho(x, y, t) > 0$ denotes the density, $u(x, y, t)$ and $v(x, y, t)$ in \mathbb{R} are the velocities and $E(x, y, t) > 0$ is the total energy. The pressure law $p(\rho, e) : \mathbb{R}^+ \times \mathbb{R}^+ \rightarrow \mathbb{R}^+$ is given by a general function such that

$$p \partial_e p + \rho^2 \partial_\rho p > 0,$$

in order to enforce the system (1.1) to be hyperbolic. The quantity $e(x, y, t) > 0$ stands for the internal energy such that

$$E = \rho e + \rho \frac{u^2 + v^2}{2}.$$

The first author was supported by the project ANR-19-CE46-0004-03 MUFFIN.

All the authors thank DAAD Procope and also the Bayerische Französische Hochschulzentrum for partially supporting this work.

The characteristic nature of the flow is governed by dimensionless quantities like the Mach number M which controls the ratio of the velocity versus the sound speed. In this work, we consider solutions in regimes only governed by the Mach number M . Hence, we rewrite the system (1.1) in a non-dimensionalized form. Arguing standard rescaling (see [16],[26],[1]), we get the following set of equations where the Mach number M stands for a given parameter:

$$\begin{cases} \rho_t + (\rho u)_x + (\rho v)_y = 0, \\ (\rho u)_t + \left(\rho u^2 + \frac{p}{M^2}\right)_x + (\rho uv)_y = 0, \\ (\rho v)_t + (\rho vu)_x + \left(\rho v^2 + \frac{p}{M^2}\right)_y = 0, \\ E_t + (u(E+p))_x + (v(E+p))_y = 0, \end{cases} \quad (1.2)$$

with the following definition for the total energy:

$$E = \rho e + M^2 \rho \frac{u^2 + v^2}{2}. \quad (1.3)$$

To shorten notations, we introduce

$$w = \begin{pmatrix} \rho \\ \rho u \\ \rho v \\ E \end{pmatrix}, \quad f(w) = \begin{pmatrix} \rho u \\ \rho u^2 + \frac{p}{M^2} \\ \rho uv \\ u(E+p) \end{pmatrix}, \quad g(w) = \begin{pmatrix} \rho v \\ \rho uv \\ \rho v^2 + \frac{p}{M^2} \\ v(E+p) \end{pmatrix}, \quad (1.4)$$

so that the system (1.2) can be written in the following compact form:

$$w_t + f(w)_x + g(w)_y = 0. \quad (1.5)$$

The system (1.2)-(1.3) is associated with the following set of physical admissible states:

$$\Omega_M = \{w \in \mathbb{R}^4; \rho > 0, e > 0\}. \quad (1.6)$$

From now on, let us emphasize that the nature of the system (1.2)-(1.3) may drastically change depending to the values of M . Indeed, with large values of M , we have to deal with a hyperbolic system while the problem becomes elliptic in the limit of M to zero. In the case of a barotropic model, i.e. the pressure law does not depend on the internal energy e , Klainermann and Majda [21] established that the compressible model tends to the incompressible counterpart given by

$$\begin{cases} u_t + uu_x + vv_y + \bar{p}_x = 0, \\ v_t + uv_x + vv_y + \bar{p}_y = 0, \\ u_x + v_y = 0, \\ \rho = \text{const}. \end{cases} \quad (1.7)$$

This is a remarkable result, since the limit pressure now satisfies the following elliptic equation:

$$\Delta \bar{p} = -(uu_x + vv_y)_x - (uv_x + vv_y)_y.$$

Next, considering the full Euler system (1.2)-(1.3), the limit behavior is proven in [13]. In the limit of M to 0, the incompressible model is recovered in a sense to be prescribed, and both kinetic and internal energies are proved to be thus conserved quantities.

In this work, we are interested to approximate solutions which are in the low Mach number regime, i.e. $M \ll 1$, as well as in the high Mach number regime. While standard upwind finite volume schemes produce good approximation with large value of M , it has been shown that they often lack in accuracy within the low Mach number regime (for instance, see [11, 16, 33]). More precisely, in the low Mach number regime, standard upwind schemes suffer from excessive numerical diffusion. For instance, the Roe scheme [29] introduces a diffusion which scales as $1/M$. As a consequence, the numerical viscosity

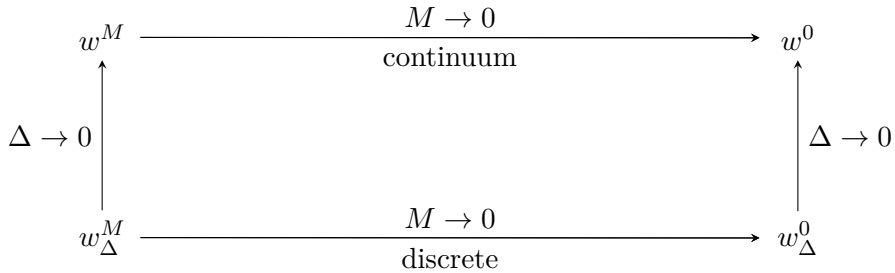


FIGURE 1.1. Asymptotic Preserving Diagram: w^M is a solution of system (1.2)-(1.3) and w^0 is a solution to (1.7) and w^M_Δ and w^0_Δ are discrete approximations to the respective solutions.

dominates the approximate solution as soon as the Mach number is close to zero (see [33, 35, 26]). To cure such a failure, a wide range of preconditioners have been developed to modify the diffusion matrix of upwind schemes. In the present paper, we will also address this issue in our design of a low Mach number scheme.

To avoid these drastic numerical errors, several approaches have been developed to design low Mach number schemes. The first concept we want to mention is the so called asymptotic preserving schemes. In fact, the limit behavior depends on the parameter M . The numerical scheme in turn should be consistent with this limit behavior according to the governing parameter. In this case, a discretization for the compressible Euler equations should tend, in a prescribed sense, to a discretization of the incompressible Euler equations when M tends to zero (see Figure 1.1).

A distinct widely used approach to deal with this problem is to split the stiff and non-stiff terms in the system (1.2)-(1.3) and discretize them in different ways to ensure the stability of the scheme. This leads to the well-known IMEX approach (for example, see [3, 27, 19, 17, 10, 4, 12]). In general, the stiff part of system (1.2)-(1.3) is strongly related to the pressure term and therefore these splitting approaches often fall in the spirit of Klein [22]. Here, we also make use of this approach and a split of the pressure term into fast and slow fluctuations is proposed.

Finally, we want to emphasize on a particular analysis of the scaling of the dependent variables in the low Mach number regime (for instance, see [11, 16, 15] and references therein). These computations give a constraint on the scaling of the different variables with respect to the Mach number in order to achieve the incompressible limit equations. For the sake of clarity, we briefly review these computations.

Within the low Mach number regime, the unknowns can be rescaled according to M as follows:

$$\rho = \rho_0 + M\rho_1, \quad u = u_0 + Mu_1, \quad v = v_0 + Mv_1, \quad e = e_0 + Me_1, \quad (1.8)$$

where, to simplify the notations, we have omitted both space (x, y) and time t dependencies.

For instance, under open boundary assumptions, from (1.2)-(1.3), we deduce that the zero-order terms satisfy

$$\nabla \rho_0 = 0 \quad \text{and} \quad \nabla \cdot \begin{pmatrix} u_0 \\ v_0 \end{pmatrix} = 0, \quad (1.9)$$

while the pressure law must verify

$$p = p_0 + M^2 p_2 \quad \text{and} \quad \nabla p_0 = 0. \quad (1.10)$$

It is worth noticing that the space dependent zero-order velocities (u_0, v_0) satisfy the free divergence condition (1.9) but they satisfy

$$\partial_x u_0 = O(1) \quad \text{and} \quad \partial_y v_0 = O(1). \quad (1.11)$$

This remark will be essential in the sequel when studying the asymptotic behavior of numerical viscosity.

As strongly underlined in [11, 16, 15], standard upwind schemes generally violate the expected scaling of the pressure. For instance, the Roe scheme [29] introduces pressure fluctuations of order $O(M)$. This leads to excessive numerical diffusion and therefore the incompressible limit might not be achieved as well.

According to (1.9) and (1.10), we define a set of asymptotic preserving states as follows:

$$\Omega_0 = \left\{ w_0 \in \mathbb{R}^4; \nabla \rho_0 = 0, p = p_0 + M^2 p_2, \nabla p_0 = 0, \nabla \cdot \begin{pmatrix} u_0 \\ v_0 \end{pmatrix} = 0 \right\}. \quad (1.12)$$

In order to produce physical relevant results, we naturally demand that Ω_0 is an invariant region for the designed upwind scheme. Moreover, we can strengthen the definition of the invariant region by combining (1.6) and (1.12) to get

$$\Omega = \Omega_M \cap \Omega_0, \quad (1.13)$$

and by imposing Ω to be an invariant region. In other words, we enforce the derived relaxation up-wind scheme to preserve Ω , to control the numerical diffusion according to the Mach number fluctuations, and to recover the correct asymptotic incompressible regime.

The present work is structured as follows. In section 2, for the sake of completeness, we recall the numerical framework of the Godunov-type scheme [18]. Next, we design a Suliciu relaxation model according to the usual approach [31, 32, 2, 8]. Unfortunately, the usual approach does not yield to the required numerical viscosity as soon as the Mach number is small enough. To correct such a failure, in section 3, we introduce a suitable Suliciu relaxation model where fast and slow phenomenon are relevantly split. The scheme obtained thus is proved to satisfy the required properties in the limit of the Mach number to zero. Finally, in section 4 we give numerical results to show the applicability of the scheme.

2. Numerical Scheme

Since the Euler system (1.2)-(1.3) under consideration is known to be invariant by Galilean rotations, we here describe the discretization of the associated 1D model given by

$$w_t + f(w)_x = 0, \quad (2.1)$$

where w and $f(w)$ are defined by (1.4). Let us underline that the 2D extension turns out to be obvious (for instance, see [14, 28]).

In the present work, we adopt a finite volume scheme of Godunov-type [18]. To address such an issue, the space is discretized by considering an uniform mesh made of cells $(x_{i-\frac{1}{2}}, x_{i+\frac{1}{2}})$ of constant size Δx . In addition, we adopt a constant time step Δt such that $t^n = n\Delta t$.

At time t^n , we define the following piecewise constant function:

$$w^n(x, t^n) = w_i^n, \quad x \in (x_{i-\frac{1}{2}}, x_{i+\frac{1}{2}}) \quad \text{for all } i \in \mathbb{Z},$$

to be an approximation of the solution of (2.1). Next, this approximation is evolved to get an updated approximation at time $t^n + \Delta t$. According to the pioneer work by Harten, Lax and van Leer [18], we introduce $\tilde{w}_{\mathcal{R}}(x/t; w_L, w_R)$ an approximate Riemann solver in the form

$$\tilde{w}_{\mathcal{R}} \left(\frac{x}{t}; w_L, w_R \right) = \begin{cases} w_L & \text{if } \frac{x}{t} < \lambda_L(w_L, w_R), \\ w^* \left(\frac{x}{t}; w_L, w_R \right) & \text{if } \lambda_L(w_L, w_R) < \frac{x}{t} < \lambda_R(w_L, w_R), \\ w_R & \text{if } \frac{x}{t} > \lambda_R(w_L, w_R), \end{cases} \quad (2.2)$$

which satisfies the following integral consistency condition:

$$\frac{1}{\Delta x} \int_{-\frac{\Delta x}{2}}^{\frac{\Delta x}{2}} \tilde{w}_{\mathcal{R}} \left(\frac{x}{\Delta t}; w_L, w_R \right) dx = \frac{1}{2} (w_L + w_R) - \frac{\Delta t}{\Delta x} (f(w_R) - f(w_L)). \quad (2.3)$$

Equipped with this approximate Riemann solver, we evolve $w^n(x, t^n + t)$ in time as follows:

$$w^n(x, t^n + t) = \tilde{w}_{\mathcal{R}} \left(\frac{x - x_{i+\frac{1}{2}}}{t}; w_i^n, w_{i+1}^n \right), \\ x \in \left(x_{i+\frac{1}{2}} - \frac{\Delta x}{2}, x_{i+\frac{1}{2}} + \frac{\Delta x}{2} \right) \quad \text{for all } i \in \mathbb{Z}.$$

From now on, let us emphasize that this time evolution is nothing but the juxtaposition of the approximate Riemann solvers stated at each interface $x_{i+\frac{1}{2}}$ for all i in \mathbb{Z} . In order to avoid interactions between all the approximate Riemann solvers, we impose the following CFL-like condition:

$$\frac{\Delta t}{\Delta x} \max_{i \in \mathbb{Z}} (|\lambda_L(w_i^n, w_{i+1}^n)|, |\lambda_R(w_i^n, w_{i+1}^n)|) \leq \frac{1}{2}.$$

Now, we are able to give the updated states at time t^{n+1} as follows:

$$w_i^{n+1} = \frac{1}{\Delta x} \int_{x_{i-\frac{1}{2}}}^{x_{i+\frac{1}{2}}} w^n(x, t^n + \Delta t) dx.$$

According to the integral consistency condition (2.3), the updated states rewrite

$$w_i^{n+1} = w_i^n - \frac{\Delta t}{\Delta x} (f(w_i^n, w_{i+1}^n) - f(w_{i-1}^n, w_i^n)). \quad (2.4)$$

Furthermore, let us underline that the functions λ_L and λ_R may depend on the Mach number M and such a CFL condition may become very restrictive as soon as M goes to zero. As a consequence, an implicit time discretization will be adopted to perform numerical simulations. The time implicit scheme therefore reads

$$w_i^{n+1} = w_i^n - \frac{\Delta t}{\Delta x} (f(w_i^{n+1}, w_{i+1}^{n+1}) - f(w_{i-1}^{n+1}, w_i^{n+1})), \quad (2.5)$$

where the numerical flux function is given by

$$f(w_L, w_R) = f(\tilde{w}_{\mathcal{R}}(0; w_L, w_R)). \quad (2.6)$$

Now, the main objective is to derive a relevant approximate Riemann solver $\tilde{w}_{\mathcal{R}}$. To access such an issue, we suggest to consider the usual Suliciu relaxation approach [8, 5, 31, 32] where the nonlinear pressure p is substituted by a new variable π . This new variable π is governed by the following equation:

$$\pi_t + u\pi_x + \frac{c^2}{\rho} u_x = \frac{1}{\epsilon} (p - \pi). \quad (2.7)$$

The relaxation parameter c is fixed according to some stability and robustness properties. As a consequence, the Suliciu relaxation model now reads

$$\begin{cases} \rho_t + (\rho u)_x = 0, \\ (\rho u)_t + \left(\rho u^2 + \frac{\pi}{M^2} \right)_x = 0, \\ (\rho v)_t + (\rho uv)_x = 0, \\ E_t + (u(E + \pi))_x = 0, \\ (\rho \pi)_t + (\rho u \pi + c^2 u)_x = \frac{\rho}{\epsilon} (p - \pi). \end{cases} \quad (2.8)$$

Let us notice that, in the limit of ϵ to zero, formally the relaxation source term implies that π converges to the expected pressure law p and then the sub-system extracted from (2.8) to govern w coincides with the expected Euler model (2.1).

For the sake of simplicity in the notations, let us set

$$U = {}^t(\rho, \rho u, \rho v, E, \rho \pi).$$

Moreover, let us note $(2.8)_{\epsilon=\infty}$ the homogeneous system extracted from (2.8). Now, we are interested in the derivation of the Riemann solution associated with $(2.8)_{\epsilon=\infty}$. First, in the following result, we give the nature of each field. The proof of this result is standard (for instance, see [14]) and it is omitted here.

Lemma 2.1. *The homogeneous system extracted from (2.8) is hyperbolic with eigenvalues $\lambda_{\pm} = u \pm \frac{\rho}{cM}$ and $\lambda_c = u$, where λ_c has multiplicity three. All the fields are linearly degenerated.*

Now, we consider an initial data given by

$$U(x, t = 0) = \begin{cases} U_L & \text{if } x < 0, \\ U_R & \text{if } x > 0. \end{cases} \quad (2.9)$$

According to Lemma 2.1, the Riemann solution of $(2.8)_{\epsilon=\infty}$ consists of piecewise constant states separated by contact discontinuities in the following form:

$$U_{\mathcal{R}}\left(\frac{x}{t}; U_L, U_R\right) = \begin{cases} U_L & \text{if } \frac{x}{t} < \lambda_-, \\ U_L^* & \text{if } \lambda_- < \frac{x}{t} < \lambda_c, \\ U_R^* & \text{if } \lambda_c < \frac{x}{t} < \lambda_+, \\ U_R & \text{if } \frac{x}{t} > \lambda_+, \end{cases} \quad (2.10)$$

where the intermediate states are given by (see [5, 6])

$$\begin{aligned} \pi_C &= \pi_L^* = \pi_R^* = \frac{\pi_L + \pi_R}{2} - cM \frac{u_R - u_L}{2}, \\ u_C &= u_L^* = u_R^* = \frac{u_L + u_R}{2} - \frac{\pi_R - \pi_L}{2cM}, \\ \rho_L^* &= \frac{1}{\frac{1}{\rho_L} + \frac{\pi_C - \pi_L}{c^2}}, & \rho_R^* &= \frac{1}{\frac{1}{\rho_R} + \frac{\pi_R - \pi_C}{c^2}}, \\ e_L^* &= e_L - \frac{\pi_L^2 - \pi_C^2}{2c^2}, & e_R^* &= e_R - \frac{\pi_R^2 - \pi_C^2}{2c^2}, \\ v_L^* &= v_L, & v_R^* &= v_R, \end{aligned} \quad (2.11)$$

with the internal energy e defined by (1.3).

From (2.10) and (2.11), we now give the Suliciu relaxation approximate Riemann solver needed to fully define the scheme (2.4)-(2.6). Let us introduce

$$U^{eq}(w) = {}^t(\rho, \rho u, \rho v, E, \rho p(\rho, e)),$$

to define the required approximate Riemann solver as follows:

$$\tilde{w}_{\mathcal{R}}\left(\frac{x}{\Delta t}; w_L, w_R\right) = U_{\mathcal{R}}\left(\frac{x}{t}; U^{eq}(w_L), U^{eq}(w_R)\right). \quad (2.12)$$

In order to exhibit the behavior of the numerical diffusion within the asymptotic regime in the limit of M to zero, we enforce the Mach number rescaling given in (1.8). We consider $w_0 \in \Omega_0$ to write

$$w_L = w_{0,L} + O(M) \quad \text{and} \quad w_R = w_{0,R} + O(M).$$

Next, since $\nabla\rho_0 = 0$ from (1.9), with no restriction we can assume that $\rho_{0,L} = \rho_{0,R} = \rho_0$. Similarly, from (1.10), we have $\nabla p_0 = 0$ and then we can assume $p_{0,L} = p_{0,R} = p_0$ and $e_{0,L} = e_{0,R} = e_0$. As a consequence, we have

$$\begin{aligned}\rho_L &= \rho_0 + O(M), & \rho_R &= \rho_0 + O(M), \\ u_L &= u_{0,L} + O(M), & u_R &= u_{0,R} + O(M), \\ v_L &= v_{0,L} + O(M), & v_R &= v_{0,R} + O(M), \\ e_L &= e_0 + O(M), & e_R &= e_0 + O(M), \\ \pi_L &= p_0 + O(M^2), & \pi_R &= p_0 + O(M^2).\end{aligned}\tag{2.13}$$

Because of (1.11), it is worth noticing that

$$u_{0,R} - u_{0,L} = O(1).\tag{2.14}$$

These expressions are now adopted to exhibit the behavior of the intermediate states U_L^* and U_R^* . First, let us focus on the intermediate pressure π_C defined by (2.11). According to (2.13), we obtain

$$\pi_C = \left(p_0 + O(M^2)\right) - \frac{cM}{2} (u_{0,R} - u_{0,L} + O(M)).\tag{2.15}$$

Arguing (2.14), we easily have

$$\pi_C = p_0 + O(M).\tag{2.16}$$

We immediately notice that the intermediate pressure π_C admits variations of the order $O(M)$ instead of variations of the order $O(M^2)$.

Concerning the other quantities, once again from (2.11) and (2.13), we get

$$\begin{cases} u_C = \frac{u_{0,L} + u_{0,R}}{2} + O(M), \\ v_L^* = v_{0,L} + O(M), & v_R^* = v_{0,R} + O(M), \\ \rho_L^* = \rho_0 + O(M), & \rho_R^* = \rho_0 + O(M), \\ e_L^* = e_0 + O(M), & e_R^* = e_0 + O(M). \end{cases}\tag{2.17}$$

Equipped with the behavior of the approximate Riemann solver, we are now able to exhibit the numerical viscosity. Let us remark that the numerical flux function rewrites

$$f(w_L, w_R) = \frac{1}{2}(f(w_L) + f(w_R)) - \frac{1}{2}D(w_R - w_L),$$

where D stands for the sought numerical diffusion matrix. Using the scaling (2.16) and (2.17), and plugging them into both exact and numerical flux functions, we obtain

$$\begin{aligned}\frac{1}{2}D(w_R - w_L) &= \frac{1}{2}(f(w_L) + f(w_R)) - f(w_L, w_R), \\ &= \begin{pmatrix} \rho_0 u_{0,L/R} + O(1) \\ \rho_0 u_{0,L/R}^2 + \frac{p_0}{M^2} + O(1) \\ \rho_0 u_{0,L/R} v_{0,L/R} + O(1) \\ u_{0,L/R}(E_0 + p_0) + O(1) \end{pmatrix} - \begin{pmatrix} \rho_0 u_{0,L/R} + O(1) \\ \rho_0 u_{0,L/R}^2 + \frac{p_0}{M^2} + O(\frac{1}{M}) \\ \rho_0 u_{0,L/R} v_{0,L/R} + O(1) \\ u_{0,L/R}(E_0 + p_0) + O(1) \end{pmatrix}, \\ &= \begin{pmatrix} O(1) \\ O(\frac{1}{M}) \\ O(1) \\ O(1) \end{pmatrix}.\end{aligned}\tag{2.18}$$

Therefore we can expect excessive diffusion in the momentum orthogonal to the interface in the low Mach number regime. As a consequence, the standard Suliciu relaxation scheme turns out to be non-relevant to approximate solutions in the low Mach number regime.

At this level, let us underline that the main failure in deriving the Suliciu relaxation solver stays in (2.14). Indeed, as soon as $u_{0,R} - u_{0,L} = O(M)$, we immediately recover the required behavior of the diffusion matrix. Such a good situation is satisfied for fully 1D simulations. Of course, we are here considering 2D problems and, unfortunately, the condition (2.14) holds true.

We have thus seen that the standard version of the Suliciu relaxation is not suited for approximating low Mach number flows in more than one space dimension. However, we also conclude, that the main problem is in the scaling of the intermediate relaxation pressure π_C . Since this relaxation technique relies on controlling a relaxation pressure, it seems natural to search for a different control of the relaxation pressure in order to achieve the asymptotic behavior of the intermediate states. This is the purpose of the next section.

3. All Mach number Relaxation Model

To cure the deficiencies of the model presented in section 2, we now propose a different relaxation model capable to accurately capture low Mach number flows. We follow the spirit of Klein et al. [23] by adopting a splitting of the pressure into a slow dynamics pressure and a fast acoustics pressure.

We suggest to decompose the scaled pressure as follows:

$$\frac{p}{M^2} = \frac{M_{loc}^2}{M^2} p + \frac{1 - M_{loc}^2}{M^2} p, \quad (3.1)$$

where $M_{loc} \in [0, 1]$ denotes a given parameter. From a practical point of view, M_{loc} will be defined as a local Mach number derived from local flow properties. Of course, with $M \leq 1$, $M_{loc} = M$ is a relevant choice but, according to numerical simulations of interest, it is more convenient to consider M_{loc} as a free parameter.

In (3.1), the quantity $\frac{M_{loc}^2}{M^2} p$ corresponds to the slow dynamics pressure while $\frac{1 - M_{loc}^2}{M^2} p$ stands for the fast acoustics pressure. Now, in the spirit of the standard Suliciu relaxation approach, we substitute both slow and fast pressures by new unknowns. We thus introduce $\frac{M_{loc}^2}{M^2} \pi$ and $\frac{1 - M_{loc}^2}{M^2} \psi$, the new variables, to respectively represent the slow and fast pressures. As a consequence, the momentum equation in (2.1) is here substituted by

$$(\rho u)_t + \left(\rho u^2 + \frac{M_{loc}^2}{M^2} \pi + \frac{1 - M_{loc}^2}{M^2} \psi \right)_x = 0.$$

Next, evolution laws satisfied by the new unknowns π and ψ must be proposed. Since the usual Suliciu relaxation model is relevant for slow dynamics pressure, we adopt the equation (2.7) to govern π . In fact, the situation turns out to be more delicate to evolve the unknown ψ . Indeed, adopting (2.7) to evolve ψ yields to non-relevant diffusion terms in the full numerical scheme. To correct such a failure, we adopt the following evolution law:

$$\psi_t + u \psi_x + \frac{c^2}{\rho} \bar{u}_x = \frac{1}{\epsilon} (p - \psi), \quad (3.2)$$

where \bar{u} coincides with a relaxed velocity governed as follows:

$$\bar{u}_t + u \bar{u}_x + \frac{1}{\rho M_{loc}^2 M^2} \psi_x = \frac{1}{\epsilon} (u - \bar{u}). \quad (3.3)$$

We are now able to give the all Mach number Suliciu relaxation model of interest in the present work

$$\left\{ \begin{array}{l} \rho_t + (\rho u)_x = 0, \\ (\rho u)_t + \left(\rho u^2 + \frac{M_{loc}^2}{M^2} \pi + \frac{1 - M_{loc}^2}{M^2} \psi \right)_x = 0, \\ (\rho v)_t + (\rho v u)_x = 0, \\ E_t + (u(E + M_{loc}^2 \pi + (1 - M_{loc}^2) \psi))_x = 0, \\ (\rho \pi)_t + (\rho u \pi + c^2 u)_x = \frac{\rho}{\epsilon} (p - \pi), \\ (\rho \psi)_t + (\rho u \psi + c^2 \bar{u})_x = \frac{\rho}{\epsilon} (p - \psi), \\ (\rho \bar{u})_t + \left(\rho u \bar{u} + \frac{1}{M_{loc}^2 M^2} \psi \right)_x = \frac{\rho}{\epsilon} (u - \bar{u}). \end{array} \right. \quad (3.4)$$

Once again, let us emphasize that in the limit of ϵ to zero, the relaxed unknowns π , ψ and \bar{u} respectively converges, at least formally, to p , p and u . As a consequence, the evolution laws for $(\rho, \rho u, \rho v, E)$ in (3.4) coincide to the initial system (2.1).

To simplify the notation in the sequel, we set

$$W = {}^t(\rho, \rho u, \rho v, E, \rho \pi, \rho \psi, \rho \bar{u}) \quad \text{and} \quad W^{eq}(w) = {}^t(\rho, \rho u, \rho v, E, \rho p, \rho p, \rho u). \quad (3.5)$$

3.1. Stability of the relaxation system

After Whitham [36] (see also [7, 28, 2]), both equilibrium system (2.1) and relaxation model (3.4) have to satisfy some compatibility conditions to prevent instabilities in the limit of ϵ to zero. These compatibility conditions are the so-called sub-characteristic conditions [36] to be put on the relaxation parameter c . In order to exhibit these restriction on c , several approaches have been proposed in the literature (for instance, see [7, 28, 2]). In the present work, we study the viscous asymptotic equilibrium system, in the limit of ϵ to zero, coming from a formal Chapman-Enskog expansion. To address such an issue, let us consider a small perturbation W^ϵ of a local equilibrium $w \in \Omega_M$ such that

$$\begin{aligned} \pi^\epsilon &= p(\rho, e) + \epsilon \pi^1 + O(\epsilon^2), \\ \psi^\epsilon &= p(\rho, e) + \epsilon \psi^1 + O(\epsilon^2), \\ \bar{u}^\epsilon &= u + \epsilon u^1 + O(\epsilon^2). \end{aligned} \quad (3.6)$$

By substituting (3.6) into (3.4) and neglecting higher order terms in ϵ , we get the following viscous equilibrium system (see Theorem 3.1):

$$w_t + f(w)_x = \epsilon (\mathcal{D}(w) w_x)_x, \quad (3.7)$$

where the flux function f is defined by (1.4) and \mathcal{D} is a diffusion matrix.

Here, the stability requirement is obtained imposing the eigenvalues of \mathcal{D} to be non-negative. In the next statement, we establish that such stability condition is verified as long as a sub-characteristic condition holds.

Theorem 3.1. *Assume that the relaxation parameter c satisfies the following sub-characteristic condition:*

$$c^2 > \rho^2 \partial_\rho p(\rho, e). \quad (3.8)$$

Then, the diffusion matrix in (3.7) has non-negative eigenvalues. As a consequence, the relaxation system (3.4) is a stable diffusive approximation of system (1.2)-(1.3).

Proof. Adopting the Chapman-Enskog expansion (3.6), we evaluate the first-order correctors π^1 , ψ^1 and \bar{u}^1 . First, from (3.4), we immediately get

$$\begin{aligned}\pi^\epsilon &= p - \epsilon \left(\pi_t^\epsilon + u\pi_x^\epsilon + \frac{c^2}{\rho}u_x \right), \\ \psi^\epsilon &= p - \epsilon \left(\psi_t^\epsilon + u\psi_x^\epsilon + \frac{c^2}{\rho}u_x \right), \\ \bar{u}^\epsilon &= u - \epsilon \left(\bar{u}_t^\epsilon + u\bar{u}_x^\epsilon + \frac{1}{\rho M_{loc}^2 M^2} \psi_x^\epsilon \right).\end{aligned}$$

Substituting the expansions (3.6) into the above three relations, we obtain

$$\begin{aligned}\pi^\epsilon &= p - \epsilon \left(p_t + up_x + \frac{c^2}{\rho}u_x \right) + O(\epsilon^2), \\ \psi^\epsilon &= p - \epsilon \left(p_t + up_x + \frac{c^2}{\rho}u_x \right) + O(\epsilon^2), \\ \bar{u}^\epsilon &= u - \epsilon \left(u_t + uu_x + \frac{c^2}{\rho M_{loc}^2 M^2} p_x \right) + O(\epsilon^2).\end{aligned}\tag{3.9}$$

Next, from both conservation of mass and momentum in (3.4), a formal computation gives

$$\begin{aligned}p_t + up_x &= -\rho \partial_\rho p u_x, \\ u_t + uu_x &= -\frac{p_x}{\rho M^2}.\end{aligned}$$

Let us plug these relations into (3.9) to write

$$\begin{aligned}\pi^1 &= -\left(\frac{c^2}{\rho} - \rho \partial_\rho p \right) u_x + O(\epsilon), \\ \psi^1 &= -\left(\frac{c^2}{\rho} - \rho \partial_\rho p \right) u_x + O(\epsilon), \\ \bar{u}^1 &= -\left(\frac{1}{M_{loc}^2} - 1 \right) \frac{1}{\rho M^2} p_x + O(\epsilon).\end{aligned}$$

Equipped with these first-order correctors, both momentum and energy equations now read

$$\begin{aligned}(\rho u)_t + \left(\rho u^2 + \frac{p}{M^2} \right)_x &= \epsilon \left(\frac{1}{\rho M^2} (c^2 - \rho^2 \partial_\rho p) u_x \right)_x + O(\epsilon^2), \\ E_t + (u(E + p))_x &= \epsilon \left(\frac{1}{\rho} (c^2 - \rho^2 \partial_\rho p) \left(\frac{u^2}{2} \right)_x \right)_x + O(\epsilon^2).\end{aligned}$$

By neglecting higher order terms in ϵ , we recover the viscous system (3.7) for a diffusion matrix given by

$$\mathcal{D} = \begin{pmatrix} 0 & 0 & 0 & 0 \\ -\frac{u}{\rho^2 M} (c^2 - \rho^2 \partial_\rho p) & \frac{1}{\rho^2 M} (c^2 - \rho^2 \partial_\rho p) & 0 & 0 \\ 0 & 0 & 0 & 0 \\ -\frac{u^2}{\rho^2} (c^2 - \rho^2 \partial_\rho p) & \frac{u}{\rho^2 M} (c^2 - \rho^2 \partial_\rho p) & 0 & 0 \end{pmatrix}.$$

The eigenvalues of \mathcal{D} easily read 0 and $\frac{1}{\rho^2 M} (c^2 - \rho^2 \partial_\rho p)$ and therefore the diffusion matrix admits non-negative eigenvalues as long as the sub-characteristic condition (3.8) holds. The proof is thus achieved. \blacksquare

3.2. Properties of the primitive relaxation system

In order to complete the definition of the numerical scheme (2.4)-(2.6), we have to exhibit the Riemann solution coming from the first-order homogeneous extracted system associated to the relaxation model (3.4). In the sequel, we denote $(3.4)_{\varepsilon=\infty}$ this first-order extracted system obtained in the limit of ε to infinity.

In the next statement, we give the expected Riemann solution. Next, this solution is studied and conditions are stated in order to enforce such solutions to belong to Ω_M . In a last result, we consider the particular case of M_{loc} close to 1.

Lemma 3.2. *The first-order homogeneous system extracted from (3.4) is hyperbolic and fully linear degenerate with eigenvalues*

$$\lambda_{s\pm}(W) = u \pm \frac{cM_{loc}}{\rho M}, \quad \lambda_{f\pm}(W) = u \pm \frac{c}{\rho M_{loc}M} \quad \text{and} \quad \lambda_c(W) = u, \quad (3.10)$$

where λ_c has multiplicity 3. Moreover, the solution to the Riemann problem is composed of 7 constant states separated by 5 contact discontinuities (see Figure 3.1) as follows:

$$W_{\mathcal{R}}\left(\frac{x}{t}; W_L, W_R\right) = \begin{cases} W_L & \text{if } \frac{x}{t} < \lambda_{f-}(W), \\ W_{L^*} & \text{if } \lambda_{f-}(W) < \frac{x}{t} < \lambda_{s-}(W), \\ W_{CL} & \text{if } \lambda_{s-}(W) < \frac{x}{t} < \lambda_c(W), \\ W_{CR} & \text{if } \lambda_c(W) < \frac{x}{t} < \lambda_{s+}(W), \\ W_{R^*} & \text{if } \lambda_{s+}(W) < \frac{x}{t} < \lambda_{f+}(W), \\ W_R & \text{if } \frac{x}{t} > \lambda_{f+}(W), \end{cases} \quad (3.11)$$

where the intermediate states are given by

$$\begin{aligned}
 \psi_{L^*} &= \psi_{R^*} = \psi_{CL} = \psi_{CR} = \psi_C = \frac{\psi_L + \psi_R}{2} + cM_{loc}M \frac{\bar{u}_L - \bar{u}_R}{2}, \\
 \bar{u}_{L^*} &= \bar{u}_{R^*} = \bar{u}_{CL} = \bar{u}_{CR} = \bar{u}_C = \frac{\bar{u}_L + \bar{u}_R}{2} + \frac{\psi_L - \psi_R}{2cM_{loc}M}, \\
 \pi_{CL} &= \pi_{CR} = \pi_C = \frac{\pi_{L^*} + \pi_{R^*}}{2} + \frac{cM}{M_{loc}} \frac{(u_{L^*} - u_{R^*})}{2}, \\
 u_{CL} &= u_{CR} = u_C = \frac{u_{L^*} + u_{R^*}}{2} + \frac{M_{loc}}{cM} \frac{\pi_{L^*} - \pi_{R^*}}{2}, \\
 e_{L^*} &= e_L - \frac{M_{loc}^2}{2c^2} (\pi_L^2 - \pi_{L^*}^2 + \frac{1 - M_{loc}^2}{1 + M_{loc}^2} (\psi_L^2 - \psi_C^2)), \\
 e_{R^*} &= e_R - \frac{M_{loc}^2}{2c^2} (\pi_R^2 - \pi_{R^*}^2 + \frac{1 - M_{loc}^2}{1 + M_{loc}^2} (\psi_R^2 - \psi_C^2)), \\
 e_{CL} &= e_{L^*} - \pi_{L^*} \frac{M_{loc}^2 \pi_{L^*} + 2(1 - M_{loc}^2) \psi_C}{2c^2} + \pi_C \frac{M_{loc}^2 \pi_C + 2(1 - M_{loc}^2) \psi_C}{2c^2}, \\
 e_{CR} &= e_{R^*} - \pi_{R^*} \frac{M_{loc}^2 \pi_{R^*} + 2(1 - M_{loc}^2) \psi_C}{2c^2} + \pi_C \frac{M_{loc}^2 \pi_C + 2(1 - M_{loc}^2) \psi_C}{2c^2}, \\
 \pi_{L^*} &= \pi_L + \frac{M_{loc}^2}{1 + M_{loc}^2} (\psi_C - \psi_L), & \pi_{R^*} &= \pi_R + \frac{M_{loc}^2}{1 + M_{loc}^2} (\psi_C - \psi_R), \\
 u_{L^*} &= u_L - \frac{M_{loc}}{cM^2(1 + M_{loc}^2)} (\psi_C - \psi_L), & u_{R^*} &= u_R + \frac{M_{loc}}{cM^2(1 + M_{loc}^2)} (\psi_C - \psi_R), \\
 \rho_{L^*} &= \frac{1}{\frac{1}{\rho_L} + \frac{\pi_L - \pi_{L^*}}{c^2}}, & \rho_{R^*} &= \frac{1}{\frac{1}{\rho_R} + \frac{\pi_R - \pi_{R^*}}{c^2}}, \\
 \rho_{CL} &= \frac{1}{\frac{1}{\rho_L} + \frac{\pi_L - \pi_C}{c^2}}, & \rho_{CR} &= \frac{1}{\frac{1}{\rho_R} + \frac{\pi_R - \pi_C}{c^2}}, \\
 v_{L^*} &= v_{CL} = v_L, & v_{R^*} &= v_{CR} = v_R.
 \end{aligned} \tag{3.12}$$

From now on, let us underline that we have enforced the eigenvalues to be ordered in (3.11). Such an order will be justified in the next result devoted to the admissibility of the Riemann solutions.

In addition, from $W_{\mathcal{R}}$ defined by (3.11)-(3.12), we are now able to give the all Mach number relaxation scheme according to (2.4)-(2.6). Let us introduce

$$W^{eq}(w) = {}^t(\rho, \rho u, \rho v, E, \rho p(\rho, e), \rho p(\rho, e), \rho u).$$

Then, the approximate Riemann solver introduced in (2.4)-(2.6) is defined as follows:

$$\tilde{w}_{\mathcal{R}} \left(\frac{x}{\Delta t}; w_L, w_R \right) = W_{\mathcal{R}} \left(\frac{x}{t}; W^{eq}(w_L), W^{eq}(w_R) \right). \tag{3.13}$$

Now, we turn establishing Lemma 3.2.

Proof. In order to exhibit the algebra of the first-order extracted system (3.4) $_{\varepsilon=\infty}$, it turns out to be convenient to consider the primitive variables given by

$$V = {}^t(\rho, u, v, e, \pi, \psi, \bar{u}),$$

where the internal energy e is defined by (1.3). Then, V is solution of the system

$$V_t + A(V)V_x = 0, \tag{3.14}$$

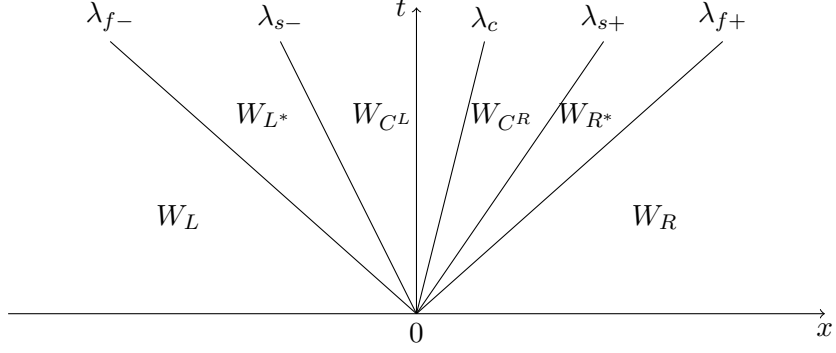


FIGURE 3.1. Wave structure of the Riemann problem

where the matrix $A(V)$ is given by

$$A(V) = \begin{pmatrix} u & \rho & 0 & 0 & 0 & 0 & 0 \\ 0 & u & 0 & 0 & \frac{M_{loc}^2}{\rho M^2} & \frac{1 - M_{loc}^2}{\rho M^2} & 0 \\ 0 & 0 & u & 0 & 0 & 0 & 0 \\ 0 & \frac{M_{loc}^2 \pi + (1 - M_{loc}^2) \psi}{\rho} & 0 & u & 0 & 0 & 0 \\ 0 & \frac{\rho}{c^2} & 0 & 0 & u & 0 & 0 \\ 0 & 0 & 0 & 0 & 0 & u & \frac{c^2}{\rho} \\ 0 & 0 & 0 & 0 & 0 & \frac{1}{\rho M^2 M_{loc}^2} & u \end{pmatrix}$$

From direct computations, we easily obtain the eigenvalues of $A(V)$ given by (3.10) with the associated eigenvectors given as follows:

- with λ_c , the eigenvectors are $r_c^1 = \begin{pmatrix} 1 \\ 0 \\ 0 \\ 0 \\ 0 \\ 0 \\ 0 \end{pmatrix}$, $r_c^2 = \begin{pmatrix} 0 \\ 0 \\ 1 \\ 0 \\ 0 \\ 0 \\ 0 \end{pmatrix}$ and $r_c^3 = \begin{pmatrix} 0 \\ 0 \\ 0 \\ 0 \\ 1 \\ 0 \\ 0 \end{pmatrix}$,

- with $\lambda_{s\pm}$, the eigenvectors are $r_{s\pm} = \begin{pmatrix} \pm \frac{\rho^2}{c M_{loc}} \\ 0 \\ c^2 \\ M_{loc}^2 \pi + (1 - M_{loc}^2) \psi \\ 0 \\ 0 \end{pmatrix}$,

- with $\lambda_{f\pm}$, the eigenvector are $r_{f\pm} = \begin{pmatrix} \rho^2 \\ \pm \frac{c}{MM_{loc}} \\ 0 \\ c^2 \\ M_{loc}^2\pi + (1 - M_{loc}^2)\psi \\ \frac{\pm c(1+M_{loc}^2)}{M_{loc}^3 M} \\ \frac{c^2(1+M_{loc}^2)}{M_{loc}^2} \end{pmatrix}$.

After a straightforward computation, we remark that $\nabla_V \lambda \cdot r = 0$ for all pairs (eigenvalue, eigenvector). As a consequence, the system (3.14) is hyperbolic fully linearly degenerated. Then, the Riemann solution is easily deduced from the Riemann invariants. Indeed, as soon as the j -th field linearly degenerated, the Riemann invariants stay constant across the j -th contact discontinuity. From standard evaluations (see [14, 8, 2, 6]), field by field, the Riemann invariants read as follows:

- associated with λ_c , the Riemann Invariants are

$$\{u, \pi, \psi, \bar{u}\},$$

- associated with $\lambda_{s\pm}$, the Riemann Invariants are

$$\left\{ u \pm \frac{cM_{loc}}{\rho M}, \pi \mp \frac{cM}{M_{loc}}u, e - \pi \frac{M_{loc}^2\pi + 2(1 - M_{loc}^2)\psi}{2c^2}, v, \psi, \bar{u} \right\},$$

- associated with $\lambda_{f\pm}$, the Riemann Invariants are

$$\left\{ \pi + \frac{c^2}{\rho}, \psi - \frac{1 + M_{loc}^2}{M_{loc}^2}\pi, \psi \mp c \frac{M(1 + M_{loc})^2}{M_{loc}}u, \psi \mp cM_{loc}M\bar{u}, e - \frac{M_{loc}^2}{2c^2}(\pi^2 + \frac{1 - M_{loc}^2}{1 + M_{loc}^2}\psi^2), v \right\}.$$

Equipped with these Riemann invariants, their continuity across their associated field yields to a linear system with solution given by (3.12). The proof is thus completed. \blacksquare

In the next statement, we establish that the Riemann solution (3.11)-(3.12) belongs to Ω_M .

Lemma 3.3. *For all $M_{loc} < 1$ such that*

$$M \notin \left(\frac{M_{loc}^2}{2 + M_{loc}^2 + \sqrt{1 - M_{loc}^4}}, \frac{M_{loc}^2}{2 + M_{loc}^2 - \sqrt{1 - M_{loc}^4}} \right), \quad (3.15)$$

there exists $c > 0$ large enough such that the Riemann solution (3.11)-(3.12) belongs to Ω_M .

From now on, let us emphasize that the condition (3.15) must be understood as a restriction to be put on M_{loc} . Here, the Mach number is never restricted. Moreover, in a low Mach number regime, the restriction to be satisfied by M_{loc} is very weak. In addition, we underline that the case $M_{loc} = M$ always satisfies (3.15), see also Figure 3.2.

Proof. The proof is established as soon as both density and internal energy are proved to be positive. Arguing the definition of the intermediate densities, given by (3.12), we immediately get the required positivity for large enough values of the relaxation parameter c .

In fact, the situation turns out to be more delicate when considering the positiveness of the intermediate internal energy. Here, we solely consider the positiveness of e_{L^*} and e_{CL} while the establishment of $e_{R^*} > 0$ and $e_{CR} > 0$ is similar.

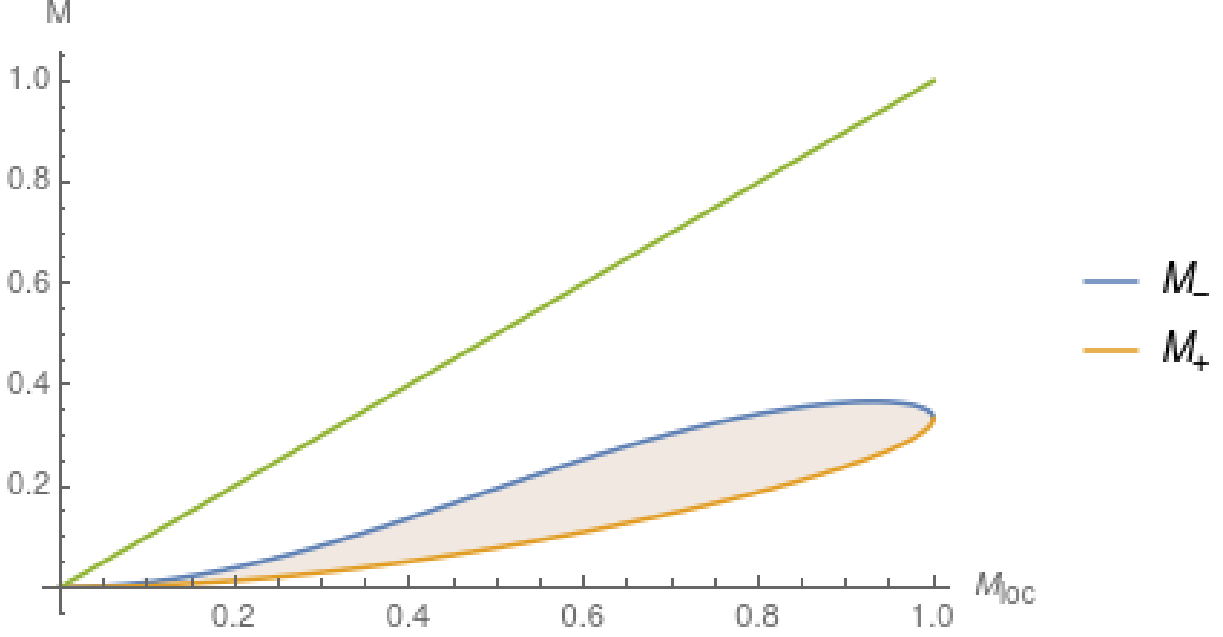


FIGURE 3.2. Functions M_{\pm} defined in (3.15). The green line gives the case $M = M_{loc}$ for reference. The condition (3.15) states that the pair (M_{loc}, M) is not inside area between the curves M_{\pm} .

Since we are considering large values of c , we suggest to rewrite the intermediate states according to an expansion with respect to c . From the intermediate state definition (3.12), we get

$$\begin{aligned}\pi_{L^*} &= c \frac{M_{loc}^3 M}{1 + M_{loc}^2} \frac{(u_L - u_R)}{2} + O(1), \\ \pi_C &= c \frac{M(1 + M_{loc}^2 + M_{loc}^4) - M_{loc}^2}{M_{loc}(1 + M_{loc}^2)} \frac{(u_L - u_R)}{2} + O(1), \\ \psi_C &= c M M_{loc} \frac{(u_L - u_R)}{2} + O(1).\end{aligned}$$

For the sake of clarity in the notations, we set

$$\begin{aligned}\theta_1 &= \frac{M_{loc}^3 M}{1 + M_{loc}^2}, \\ \theta_2 &= \frac{M(1 + M_{loc}^2 + M_{loc}^4) - M_{loc}^2}{M_{loc}(1 + M_{loc}^2)},\end{aligned}\tag{3.16}$$

in order to write

$$\begin{aligned}\pi_{L^*} &= c \theta_1 \frac{(u_L - u_R)}{2} + O(1), \\ \pi_C &= c \theta_2 \frac{(u_L - u_R)}{2} + O(1).\end{aligned}$$

According to the definition of e_{L^*} , given by (3.12), we obtain

$$e_{L^*} = e_L + M_{loc}^2 \left(\theta_1^2 + \frac{1 - M_{loc}^2}{1 + M_{loc}^2} \theta_2^2 \right) \frac{(u_L - u_R)^2}{8} + O\left(\frac{1}{c}\right).$$

With $M_{loc} \in (0, 1)$, since $e_L > 0$, we get $e_{L^*} > 0$ as soon as c is large enough. Now, the expansion of e_{CL} with respect to c reads as follows:

$$e_{CL} = e_L + f(M_{loc}, M) \frac{(u_L - u_R)^2}{8} + O\left(\frac{1}{c}\right),$$

where we have set

$$f(M_{loc}, M) = \left(M_{loc}^2 \frac{1 - M_{loc}^2}{1 + M_{loc}^2} M^2 M_{loc}^2 + M_{loc}^2 \theta_2^2 - 2(1 - M_{loc}^2) M M_{loc} (\theta_1 - \theta_2) \right).$$

The quantity e_{CL} will be proved to be positive as soon as $f(M_{loc}, M)$ is fixed non-negative. By definition of θ_1 and θ_2 , given by (3.16), we write

$$f(M_{loc}, M) = \frac{(3 + 4M_{loc}^2 + 2M_{loc}^4)M^2 - M(4M_{loc}^2 + 2M_{loc}^4) + M_{loc}^4}{(1 + M_{loc}^2)^2}.$$

Since the denominator is always positive we only have to consider the numerator as given in the following function:

$$\mathcal{N}(M_{loc}, M) = (3 + 4M_{loc}^2 + 2M_{loc}^4)M^2 - M(4M_{loc}^2 + 2M_{loc}^4) + M_{loc}^4.$$

The function \mathcal{N} is a quadratic convex function with respect to M and it admits the following roots:

$$M_{\pm} = \frac{M_{loc}^2}{2 + M_{loc}^2 \pm \sqrt{1 - M_{loc}^4}}. \quad (3.17)$$

The required non-negativity of the function $f(M_{loc}, M)$ is thus satisfied as long as M does not belong to (M_+, M_-) . The proof is achieved. \blacksquare

To conclude the presentation of the main properties satisfied by the Riemann solutions of system (3.4) $_{\varepsilon=\infty}$, we now show that such solutions coincide, in a sense to be prescribed, with the Riemann solutions of system (2.8) $_{\varepsilon=\infty}$ in the limit of M_{loc} to 1. As a consequence, the all Mach number relaxation scheme (2.4)-(2.6)-(3.13) coincides with the standard Suliciu relaxation scheme (2.4)-(2.6)-(2.12) which performs well when the flow is not in the low Mach number regime.

Lemma 3.4. *In the limit of M_{loc} to 1, the vector*

$$\tilde{U}_{\mathcal{R}}\left(\frac{x}{t}; W_L, W_R\right) = {}^t(\rho, \rho u, \rho v, E, \rho \pi),$$

extracted from the Riemann solution (3.11)-(3.12) of (3.4) $_{\varepsilon=\infty}$ tends to the vector $U_{\mathcal{R}}(\frac{x}{t}, U_L, U_R)$, defined by (2.10)-(2.11), solution of the Riemann problem associated with (2.8) $_{\varepsilon=\infty}$.

Proof. When M_{loc} tends to 1, the last two equations in (3.4) $_{\varepsilon=\infty}$ do not have any influence on the rest of the system. As a consequence, the extracted system from (3.4) $_{\varepsilon=\infty}$ to govern ${}^t(\rho, \rho u, \rho v, E, \rho \pi)$ is identical to the standard relaxation system (2.8) $_{\varepsilon=\infty}$. \blacksquare

3.3. Low Mach number properties of the new relaxation scheme

In this section, we study the properties satisfied by the derived all Mach number relaxation scheme. In fact, we are here interested in two properties. The first property of main interest is the so-called Asymptotic-Preserving property. Indeed, in the limit of M to zero, we will establish that the scheme converges to a consistent discretization of the expected incompressible model flow (1.7). The second property concerns the behavior of the numerical diffusion. Indeed, after (2.19), the numerical viscosity may become preponderant as M goes to zero by producing very large numerical error. We will show that such a failure is corrected by adopting the numerical scheme (2.4)-(2.6)-(3.13).

Within this asymptotic analysis, we adopt $M_{loc} = M$ since such a choice is relevant and satisfies the restriction (3.15). Also since the eigenvalues become very large in the low Mach number regime and therefore the CFL restriction becomes too restrictive we now adopt the implicit time stepping technique for the proposed numerical scheme.

First, we consider the AP-properties satisfied by the derived scheme. More precisely, in the limit of M to zero, we have to recover the asymptotic regime governed by (1.9)-(1.10). To address such an issue, we have to consider the full 2D-scheme as defined in (2.4)-(2.6)-(3.13). Due to the implicit time stepping the regularity of the solution at the new time-level might not be known in advance. Therefore we use the following assumption.

We assume that the expansions of the primitive variables given in (1.8) do also hold at the new time step. Moreover we assume that the discrete time derivatives for each primitive variable q scale independent of the Mach number, i.e.

$$\frac{1}{\Delta t} (q_{i,j}^{n+1} - q_{i,j}^n) = O(1). \quad (3.18)$$

Lemma 3.5. *Consider the scheme (2.4)-(2.6)-(3.13). Under the assumption (3.18), it holds that*

$$p_{i+1,j}^{n+1} - p_{i-1,j}^{n+1} = O(M^2). \quad (3.19)$$

and

$$p_{i,j+1}^{n+1} - p_{i,j-1}^{n+1} = O(M^2). \quad (3.20)$$

Proof. First, we consider the discrete equation for the x -momentum given by

$$(\rho u)_{i,j}^{n+1} = (\rho u)_{i,j}^n - \frac{\Delta t}{\Delta x} (f_{i+1/2,j}^{\rho u,n+1} - f_{i-1/2,j}^{\rho u,n+1} + g_{i,j+1/2}^{\rho u,n+1} - g_{i,j-1/2}^{\rho u,n+1}), \quad (3.21)$$

where, with clear notations to define the numerical flux function at the interface $x_{i+1/2}$, we have set

$$\begin{aligned} f_{i\pm 1/2,j}^{\rho u,n+1} &= (\rho u^2)_{i\pm 1/2,j}^{n+1} + \pi_{i\pm 1/2,j}^{n+1} + \frac{1-M^2}{M^2} \psi_{i\pm 1/2,j}^{n+1}, \\ g_{i,j\pm 1/2}^{\rho u,n+1} &= (\rho uv)_{i,j\pm 1/2}^{n+1}. \end{aligned}$$

Next, multiply (3.21) by M^2 and rearrange to get

$$\begin{aligned} \psi_{i+1/2,j}^{n+1} - \psi_{i-1/2,j}^{n+1} &= M^2(\psi_{i+1/2,j}^{n+1} - \psi_{i-1/2,j}^{n+1}) - M^2 \frac{\Delta x}{\Delta t} ((\rho u)_{i,j}^{n+1} - (\rho u)_{i,j}^n) \\ &\quad + M^2 \left((\rho u^2)_{i+1/2,j}^{n+1} + \pi_{i+1/2,j}^{n+1} - (\rho u^2)_{i-1/2,j}^{n+1} - \right. \\ &\quad \left. \pi_{i-1/2,j}^{n+1} + (\rho uv)_{i,j+1/2}^{n+1} - (\rho uv)_{i,j-1/2}^{n+1} \right). \end{aligned}$$

Under Assumption (3.18) the above relation reduces to

$$\psi_{i+1/2,j}^{n+1} - \psi_{i-1/2,j}^{n+1} = O(M^2).$$

With the definition of ψ from (3.12) and its relaxation equilibrium together again with the assumption (3.18) there is

$$\psi_{i+1/2,j}^{n+1} = \frac{p_{i+1,j}^{n+1} + p_{i,j}^{n+1}}{2} + O(M^2).$$

Therefore, we obtain

$$p_{i+1,j}^{n+1} - p_{i-1,j}^{n+1} = O(M^2).$$

By symmetry, from the equation for the y -momentum, we also have

$$p_{i,j+1}^{n+1} - p_{i,j-1}^{n+1} = O(M^2). \quad \blacksquare$$

Equipped with these computations, we are now able to state the following result.

Lemma 3.6. *Consider the scheme (2.4)-(2.6)-(3.13) and denote by N_x and N_y the number of grid points in the x and y direction respectively. Further assume that the pressure at the boundary is determined by*

$$\forall_{j \in [1, N_y]} p_{0,j}^{n+1} = p_{N_x+1,j}^{n+1} = p_0 \quad \text{and} \quad \forall_{i \in [1, N_x]} p_{i,0}^{n+1} = p_{i,N_y+1}^{n+1} = p_0. \quad (3.22)$$

Then, if at least one of N_x and N_y is even, there is

$$\forall_{i,j} p_{i,j}^{n+1} = p_0 + O(M^2). \quad (3.23)$$

Proof. Consider the case that N_x is even. From (3.19), there is for any j and any integer $k \in \{1, N_x/2\}$

$$p_{0,j}^{n+1} = p_{2k,j}^{n+1} = p_0 + O(M^2). \quad (3.24)$$

Conversely, we have

$$p_{N_x+1,j}^{n+1} = p_{2k-1,j}^{n+1} = p_0 + O(M^2). \quad (3.25)$$

Since j was arbitrary and the same argument holds if N_y is even, this concludes the proof. \blacksquare

Lemma 3.7. *Consider the scheme (2.4)-(2.6)-(3.13). Under the assumption (3.18) it holds that*

$$\operatorname{div}(u, v) = \Delta x \operatorname{div}(\operatorname{grad}(u^2, v^2)) \frac{\gamma - 1}{\gamma} \frac{\rho_0}{2c} + O(\Delta x). \quad (3.26)$$

Proof. Consider the energy equation given by

$$E_{i,j}^{n+1} = E_{i,j}^n - \frac{\Delta t}{\Delta x} \left(f_{i+1/2,j}^{E,n+1} - f_{i-1/2,j}^{E,n+1} + g_{i,j+1/2}^{E,n+1} - g_{i,j-1/2}^{E,n+1} \right), \quad (3.27)$$

where we have set

$$\begin{aligned} f_{i+1/2,j}^{E,n+1} &= (u(E + M^2\pi + (1 - M^2)\psi))_{i+1/2,j}^{n+1}, \\ g_{i,j+1/2}^{E,n+1} &= (v(E + M^2\pi + (1 - M^2)\psi))_{i,j+1/2}^{n+1}. \end{aligned}$$

We now focus on the following limit:

$$\lim_{M \rightarrow 0} (E_{i,j}^{n+1} - E_{i,j}^n) \stackrel{(1.3)}{=} \lim_{M \rightarrow 0} \left(\underbrace{\frac{p_{i,j}^{n+1}}{\gamma - 1} - \frac{p_{i,j}^n}{\gamma - 1}}_{\stackrel{(3.23)}{=} O(M^2)} + M^2 \underbrace{\left(\rho_{i,j}^{n+1} \left(\frac{u^2 + v^2}{2} \right)_{i,j}^{n+1} - \rho_{i,j}^n \left(\frac{u^2 + v^2}{2} \right)_{i,j}^n \right)}_{\stackrel{\text{assumption (3.18)}}{=} O(1)} \right) = 0. \quad (3.28)$$

Next, consider the numerical fluxes in the x -derivative. In the limit of M to 0, we get

$$f_{i+1/2,j}^{E,0} := \lim_{M \rightarrow 0} f_{i+1/2,j}^E = (u((\rho e) + \psi))_{i+1/2,j}. \quad (3.29)$$

From (3.23) and by definition of $\psi_{i+1/2,j}$ given by (3.12), we have

$$\lim_{M \rightarrow 0} \psi_{i+1/2,j} = p_0. \quad (3.30)$$

Moreover, in the low Mach number limit, the numerical flux function is defined by the intermediate centred states $C^{L,R}$ given by (3.12). As a consequence, we obtain

$$\begin{aligned}\lim_{M \rightarrow 0} u_{i+1/2,j} &= \frac{u_{0,i,j} + u_{0,i+1,j}}{2}, \\ \lim_{M \rightarrow 0} \rho_{i+1/2,j} &= \left(\rho_0 + \frac{\rho_0^2 (u_{0,i,j} - u_{0,i+1,j})}{2c + \rho_0 (u_{0,i+1,j} - u_{0,i,j})} \right), \\ \lim_{M \rightarrow 0} e_{i+1/2,j} &= \left(e_{0,i/i+1,j} + p_0 \frac{u_{0,i,j} - u_{0,i+1,j}}{2c} \right).\end{aligned}$$

Since, we reject the possibility of shocks in the low Mach number limit, therefore we have

$$\Delta_{u,i+\frac{1}{2},j} := u_{0,i,j} - u_{0,i+1,j} = O(\Delta x). \quad (3.31)$$

After performing an expansion of $\rho_{i+1/2,j}$ in $\Delta_{u,i+\frac{1}{2},j}$, up to second-order terms, we write the numerical flux as follow:

$$\begin{aligned}f_{i+1/2,j}^{E,0} &= \frac{u_{0,i,j} + u_{0,i+1,j}}{2} \left(\frac{\gamma}{\gamma-1} p_0 + \Delta_{u,i+\frac{1}{2},j} \frac{\rho_0}{2c} p_0 \right) + O(\Delta x^2), \\ &= \frac{u_{0,i,j} + u_{0,i+1,j}}{2} \frac{\gamma}{\gamma-1} p_0 - \frac{u_{0,i+1,j}^2 - u_{0,i,j}^2}{2} \frac{\rho_0}{2c} p_0 + O(\Delta x^2).\end{aligned}$$

Then we immediately get

$$\begin{aligned}f_{i+1/2,j}^{E,0} - f_{i-1/2,j}^{E,0} &= \\ &= \frac{u_{0,i+1,j} - u_{0,i-1,j}}{2} \frac{\gamma}{\gamma-1} p_0 - \frac{u_{0,i+1,j}^2 - 2u_{0,i}^2 + u_{0,i-1,j}^2}{2} \frac{\rho_0}{2c} p_0 + O(\Delta x^2).\end{aligned} \quad (3.32)$$

Since the analysis in the y -direction is analogous, from (3.28) and (3.32), we simplify (3.27) as follows:

$$\begin{aligned}0 &= -\frac{1}{\Delta x} \left(\frac{u_{0,i+1,j} - u_{0,i-1,j}}{2} \frac{\gamma}{\gamma-1} p_0 - \frac{u_{0,i+1,j}^2 - 2u_{0,i}^2 + u_{0,i-1,j}^2}{2} \frac{\rho_0}{2c} p_0 \right) \\ &\quad - \frac{1}{\Delta x} \left(\frac{v_{0,i,j+1} - v_{0,i,j-1}}{2} \frac{\gamma}{\gamma-1} p_0 - \frac{v_{0,i,j+1}^2 - 2v_{0,i,j}^2 + v_{0,i,j-1}^2}{2} \frac{\rho_0}{2c} p_0 \right) + O(\Delta x).\end{aligned}$$

According to suitable assumptions on the regularity of the dependent variables (3.31), we write

$$0 = - (u(x_i, y_j)_x + v(x_i, y_j)_y) + \Delta x \left(u(x_i, y_j)_{x,x}^2 + v(x_i, y_j)_{y,y}^2 \right) \frac{\gamma-1}{\gamma} \frac{\rho_0}{2c} + O(\Delta x).$$

Therefore, in the low Mach number limit, the energy equation (3.27) reduces to (3.26). \blacksquare

It is worth noticing that the relation (3.26) gives the divergence constraint for the velocity field with a diffusion term that vanishes in the limit of $\Delta x \rightarrow 0$.

Therefore we can now state the following Theorem on the preservation of the asymptotic set (1.12).

Theorem 3.8. *The numerical scheme defined by (2.4)-(2.6)-(3.13), under the assumptions of Lemma 3.6, preserves the asymptotic preserving set (1.12).*

Proof. The proof is a collection of the results of the Lemma 3.6 and 3.7. \blacksquare

Further we can now state the following on the limit behaviour of the numerical scheme.

Theorem 3.9. *The numerical scheme defined by (2.4)-(2.6)-(3.13), under the assumptions of Lemma 3.6, is asymptotic preserving when M tends to 0, i.e. it gives a consistent approximation of the limit equations (1.7).*

Proof. We investigate the limit of $M \rightarrow 0$ of the numerical scheme. In order to get the limit equation (1.7). The most difficult part is the divergence constraint of the velocity field, where this is proven for Lemma 3.7. Concerning the limit equations for the velocity components we rely on the fact, that the scheme is consistent with the compressible Euler equations. The equations for the velocities are just reformulations of the momenta equations of the compressible Euler equations assuming sufficient regularity of the solution. Therefore the numerical scheme is also consistent with the velocity equations of (1.7). \blacksquare

Next, motivated by the analysis on the diffusion of the standard Suliciu relaxation in section 2 in equation (2.18), let us exhibit the behavior of the numerical diffusion given by

$$D(w_R - w_L) = \frac{1}{2} (f(w_L) + f(w_R)) - f(w_L, w_R), \quad (3.33)$$

where D stands for the numerical diffusion matrix and $f(w_L, w_R)$ is the numerical flux function defined by (2.6)-(3.13).

Theorem 3.10. *Consider the numerical flux define by (2.6)-(3.13). Under the assumption (3.18) and the assumptions of Lemma 3.6 we have that*

$$D = \begin{pmatrix} O(1) \\ O(1) \\ O(1) \\ O(1) \end{pmatrix}. \quad (3.34)$$

Proof. In a first step, we adopt the rescaling (2.13) supplemented by the scaling of the new relaxation variables as follows:

$$\begin{aligned} \psi_L &= p_0 + O(M^2), & \psi_R &= p_0 + O(M^2), \\ \bar{u}_L &= u_{0,L} + O(M), & \bar{u}_R &= u_{0,R} + O(M). \end{aligned}$$

This is justified by the results of the Lemma 3.6 and 3.7. Arguing the definition of the intermediate states, given by (3.12), the following scaling of the intermediate states directly holds:

$$u_{L^*} = u_{0,L} + O(M), \quad u_{R^*} = u_{0,R} + O(M), \quad (3.35)$$

$$\rho_{L^*} = \rho_0 + O(M), \quad \rho_{R^*} = \rho_0 + O(M), \quad (3.36)$$

$$\rho_{C^L} = \rho_0 + O(1), \quad \rho_{C^R} = \rho_0 + O(1), \quad (3.37)$$

$$\pi_C = p_0 + O(1), \quad u_C = u_{0,L/R} + O(1), \quad (3.38)$$

$$\pi_{L^*} = p_0 + O(M^2), \quad \pi_{R^*} = p_0 + O(M^2), \quad (3.39)$$

$$\psi_C = p_0 + O(M^2), \quad \bar{u} = u_{0,L/R} + O(1), \quad (3.40)$$

$$e_{L^*} = e_{0,L} + O(M), \quad e_{R^*} = e_{0,R} + O(M), \quad (3.41)$$

$$e_{C^L} = e_{0,L} + O(1), \quad e_{C^R} = e_{0,R} + O(1), \quad (3.42)$$

$$v_{L^*} = v_{C^L} = v_{0,L} + O(M), \quad v_{R^*} = v_{C^R} = v_{0,R} + O(M). \quad (3.43)$$

A straightforward computation yields to the following asymptotic behavior satisfied by the numerical flux function:

$$f(w_L, w_R) = \begin{pmatrix} \rho_0 u_{0,L/R} + O(1) \\ \rho_0 u_{0,L/R}^2 + \frac{p_0}{M^2} + O(1) \\ \rho_0 u_{0,L/R} v_{0,L/R} + O(1) \\ (u_{0,L/R}(E_0 + p_0)) + O(1) \end{pmatrix}.$$

and therefore the result is achieved. \blacksquare

As a consequence, the numerical viscosity of the derived numerical scheme (2.4)-(2.6)-(3.13) does not depend on the Mach number. Put in other words, as M goes to zero, the numerical error does not dominate the simulation at the discrepancy with the standard Suliciu relaxation scheme (2.4)-(2.6)-(2.12).

4. Numerical results

Now, the proposed low Mach number scheme is tested for its practical applicability. In all test cases, an ideal gas law is used with $\gamma = \frac{5}{3}$ as well as an equidistant grid. The emphasis in these tests lies in the comparison of the new relaxation scheme with respect to the standard Suliciu relaxation scheme. By comparison between (2.11) and (3.12), it is clear that the standard scheme is recovered when choosing $M_{loc} = 1$. The new relaxation scheme is denoted as S_M while S_1 denotes the standard relaxation scheme.

In order to treat the relaxation source terms we use the relaxation projection method for the explicit and the implicit timestepping technique. I.e. the initial condition to determine the numerical flux is always considered at the relaxation equilibrium, as has been stated in the definition (2.6). For the explicit time stepping this trivially results in the fact, that none of the newly introduced relaxation variables is actually evolved in time. In the implicit timestepping case we have to solve the following system, given for the sake simplicity in a semi-discrete form,

$$W^{n+1} = W^n - \Delta_t \nabla \cdot F(W^{n+1}), \quad (4.1)$$

where the spatial derivatives have been defined in the sections 2 and 3.

Now, along the definitions of section 3, we define

$$\begin{aligned} W &= (\rho, \rho \mathbf{u}, E, \rho \pi, \rho \hat{\mathbf{u}}, \rho \psi)^t, \\ W^{eq} &= (\rho, \rho \mathbf{u}, E, \rho p, \rho \mathbf{u}, \rho p)^t, \\ QW &= (\rho, \rho \mathbf{u}, E)^t, \\ F &= (f^\rho, f^{\rho \mathbf{u}}, f^E, f^{\rho \pi}, f^{\rho \hat{\mathbf{u}}}, f^{\rho \psi})^t, \\ QW &= (f^\rho, f^{\rho \mathbf{u}}, f^E)^t, \end{aligned} \quad (4.2)$$

and solve the implicit system (4.1) only for the physical variables, i.e. we solve

$$QW^{n+1} = QW^n - \Delta_t \nabla \cdot QF(W^{n+1,eq}). \quad (4.3)$$

This highly reduces the number of unknowns in the implicit system. Moreover we like to point out that the system (4.3) is non-linear. Therefore we need to employ a Newton-Raphson iteration to find the unknown QW^{n+1} .

We implemented the respective schemes in the SLH code [25] and use the functionalities that are implemented there. In each Newton-Raphson step a linear system has to be solved. We use the PARDISO framework [9, 34, 24] to achieve this task. For higher order timestepping the implicit time integration method ESDIRK34 from [20] is used. To ensure second order in space a minmod limiter is applied to reconstruct the conserved quantities in each cell.

Even though the implicit time stepping is unconditionally stable, we introduce a time step restriction in the following form

$$\frac{\Delta_x}{\Delta_t} = \frac{1}{2} |\mathbf{u}|. \quad (4.4)$$

At last we define the definition of the parameter M_{loc} . When an implicit time-stepping is used we determine M_{loc} as

$$M_{loc,i+\frac{1}{2},j} = \min(\max(M_{loc,i,j}, M_{loc,i+1,j}), 1). \quad (4.5)$$

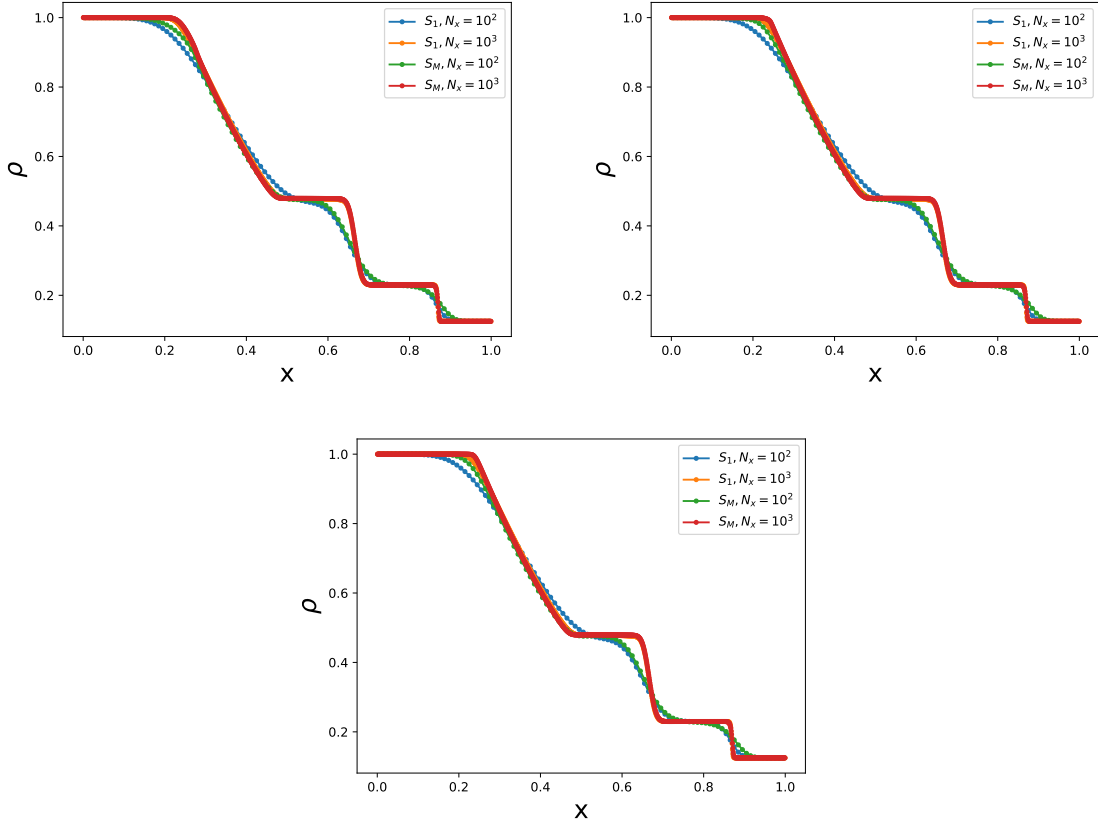


FIGURE 4.1. Numerical approximations to the Sod shock tube test for the schemes S_1 and S_M at different Mach numbers and at different resolutions at time 0.2. Top left: $M = 10^{-1}$. Top right: $M = 10^{-2}$. Bottom center: $M = 10^{-3}$.

In all the test cases, if not mentioned otherwise, the prescribed implicit timestepping procedure is used.

4.1. Sod Shock Tube test

The first test case investigates the capability of the low Mach number scheme to deal with discontinuities. To this end, the Sod shock tube test is concerned, see [30]. The computational domain is $D = [0, 1]$ and the initial conditions are set as

$$(\rho(0, x), u(0, x), p(0, x)) = \begin{cases} (1.0, 0, 1.0) & \text{if } x < 0.5, \\ (0.125, 0, 0.1) & \text{if } x > 0.5. \end{cases} \quad (4.6)$$

Only first order versions of the schemes S_1, S_M are concerned in order to investigate the influence of the numerical flux function on the approximation. Moreover, in this test case an explicit time integration is performed. Since the explicit time integration is stiff with respect to M, M_{loc} , the local Mach number has to be controlled in order for the fastest eigenvalues in (3.10) to be bounded. Therefore in this case we set $M = M_{loc}$ that also satisfies (3.15). The results are shown in Figure 4.1.

When looking at the numerical approximations with 100 cells and comparing them with the solutions on higher resolutions, a similar behaviour on all the different Mach numbers can be observed. At first, the low Mach number scheme seems to be more diffusive on the shock around 0.9. Both schemes show a comparable performance on the contact discontinuity at 0.6, while the rarefaction wave is much better captured by the low Mach number scheme. Moreover, both schemes are in good agreement in all regimes when the resolution is increased.

4.2. Gresho Vortex test

A classical test case for low Mach number properties is the Gresho vortex. The Gresho vortex is an axisymmetric steady state solution of the compressible Euler equations and the velocity field satisfies the free divergence condition from the incompressible limit. Here the modified version from [26] is considered. It is defined in polar coordinates and by axisymmetry only the radial component needs to be specified. Denoting by u_ϕ the angular velocity, it is set as

$$u_\phi(r) = \begin{cases} 5r & \text{if } 0 \leq r \leq 0.2, \\ 2 - 5r & \text{if } 0.2 \leq r \leq 0.4, \\ 0 & \text{if } 0.4 \leq r, \end{cases} \quad (4.7)$$

and the pressure distribution is given by

$$p(r) = p_0 + \begin{cases} \frac{25}{2}r^2 & \text{if } 0 \leq r \leq 0.2, \\ \frac{25}{2}r^2 + 4(1 - 5r - \ln 0.2 + \ln r) & \text{if } 0.2 \leq r \leq 0.4, \\ 4 \ln 2 - 2 & \text{if } 0.4 \leq r, \end{cases} \quad (4.8)$$

where $p_0 = \frac{\rho}{\gamma M^2}$. The density ρ is considered as constant and the computational domain is $D = [-1, 1] \times [-1, 1]$. Fixing ρ , the reference Mach number M is used to scale the vortex to different regimes. In order to see how the schemes perform on a low resolution the simulations are performed on an equidistant grid in both spatial dimensions with $N_x = N_y = 40$ and periodic boundary conditions are imposed. The resulting distributions of the relative Mach number, i.e. $M_{rel}(t, x, y) = \frac{M_{loc}(t, x, y)}{M}$, after one rotation for different reference Mach numbers are shown in Figure 4.2.

The scheme S_1 introduces an increasing amount of diffusion with decreasing Mach number; as can be seen in the top row of Figure 4.2. In contrast to that, the new relaxation scheme S_M preserves the vortex structure on all Mach numbers equally good. This result is expected from the derivations of the numerical diffusion of the upwind schemes S_1 in (2.19) and S_M in (3.34).

Another criterion to check the quality of the numerical approximation is the kinetic energy. Since the vortex is a stationary solution, the kinetic energy also remains constant in the exact solution. The evolution of the total kinetic energy in the computational domain is shown in Figure 4.3.

The scheme S_1 shows an increasing diffusion of the kinetic energy by decreasing Mach number. Even more, for Mach number 10^{-4} , the scheme actually shows also convergence problems and the solution becomes nonphysical. On the other hand the scheme S_M shows only a small diffusion of the kinetic energy and the diffusion of the total relative kinetic energy is practically identical at the different Mach numbers.

Lastly we compare the CPU times that were needed for each scheme. The algorithm is run on a single CPU of the type Intel(R) Core(TM) i5-4690 CPU with 3.50GHz on a 64-bit 4.4.176-96 linux system. The CPU times are found in Table 4.1.

As can be seen the new scheme S_M is also more efficient then the scheme S_1 . In all regimes the CPU times are significantly smaller for S_M then for S_1 . Moreover the CPU times for S_M are also stable when lower Mach number flows are concerned. However we would like to mention that the Newton-Raphson iteration has a strong impact on the CPU time. For example, slightly different termination

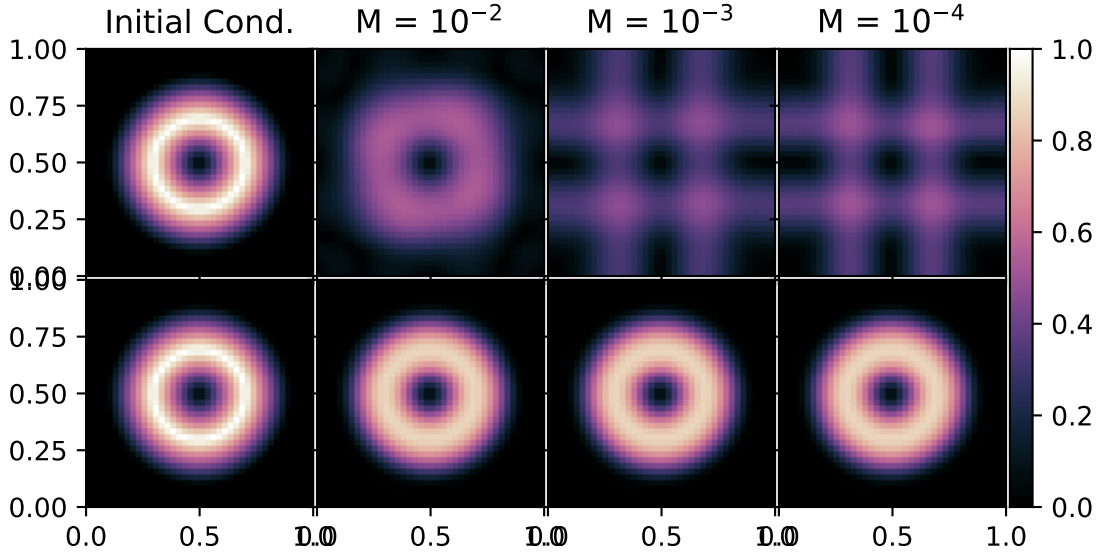


FIGURE 4.2. Local relative Mach number for the Gresho Vortex after one rotation at different Mach numbers. Top: results for the scheme S_1 . Bottom: results for the scheme S_M .

TABLE 4.1. CPU times in seconds for the Gresho vortex test for the schemes S_1 and S_M at different Mach numbers.

Scheme	Mach number		
	10^{-2}	10^{-3}	10^{-4}
S_M	124	124	120
S_1	4885	42284	184980

criteria might lead to different CPU times. This is especially true for the scheme S_1 which shows a slow convergence behaviour.

4.3. Smooth Gresho Vortex

In this test investigate the stability of the order of the numerical scheme S_M in the low Mach number regime. Since we deal with a formal second order scheme, a smooth test problem is needed. The standard Gresho vortex however does not admit a smooth distribution of the conserved quantities.

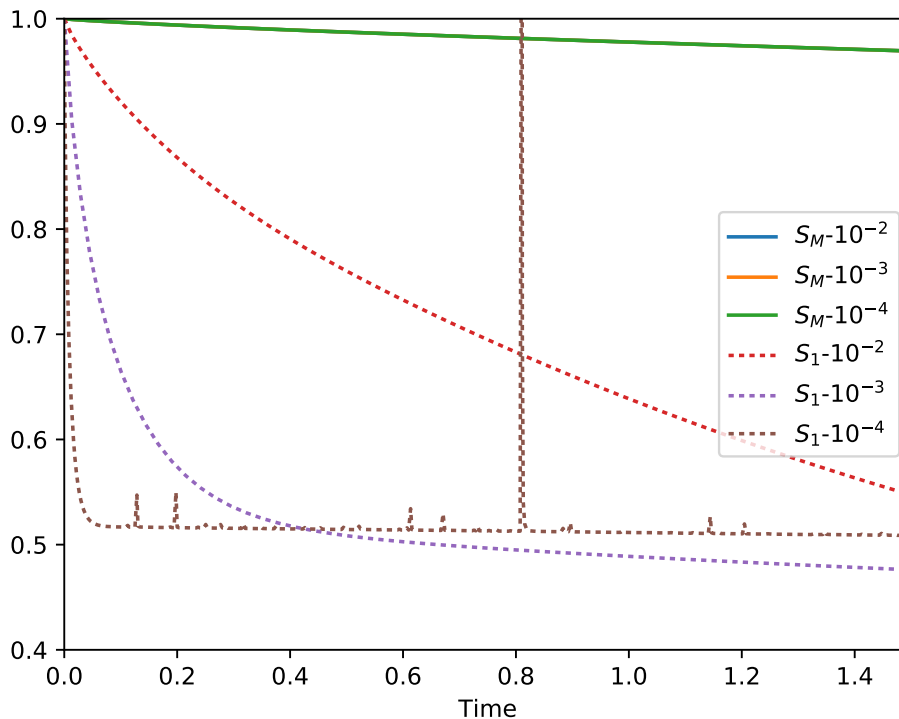


FIGURE 4.3. Evolution of the total kinetic energies in the numerical approximation of the Gresho vortex at different Mach numbers for different schemes. Shown is the relative total kinetic energy, i.e. $\frac{tKE(t)}{tKE(0)}$.

Therefore we give here a smooth version of the above described vortex. We do this by interpolating the velocity profile of the standard Gresho vortex at the points $r = 0, r = 0.2, r = 0.4$ by demanding a smooth transition across the quadrature points. The resulting distributions are now given by

$$u_\phi(r) = \begin{cases} 75r^2 - 250r^3 & \text{if } 0 \leq r \leq 0.2, \\ -4 + 60r - 225r^2 + 250r^3 & \text{if } 0.2 \leq r \leq 0.4, \\ 0 & \text{if } 0.4 \leq r, \end{cases} \quad (4.9)$$

and

$$p(r) = p_0 + \begin{cases} \frac{5625}{4}r^4 - 7500r^5 + \frac{31250}{3}r^6 & \text{if } 0 \leq r \leq 0.2, \\ \frac{602}{15} - 480r + 2700r^2 - \frac{29000}{3}r^3 + \frac{80625}{4}r^4 \\ \quad - 22500r^5 + \frac{31250}{3}r^6 + 16 \ln 5r & \text{if } 0.2 \leq r \leq 0.4, \\ 16 \ln 2 - \frac{154}{15} & \text{if } 0.4 \leq r, \end{cases} \quad (4.10)$$

We now investigate the experimental order of convergence given in table 4.2. In fact the numerical errors are practically invariant across all Mach numbers. And with this also the convergence rate is robust with respect to the flow regime and a second order convergence is achieved. The only drop in convergence rates is in the density. Here in fact the order is below 2. However the total error is really low and finite precision problems influence the convergence rates.

TABLE 4.2. L^2 error and the estimated rate of convergence (EoC) at different Mach numbers.

Res.	ρ	EoC	ρu	EoC	ρv	EoC	E	EoC
$M = 10^{-2}$								
40x40	2.93 e-06	-	1.89 e-02	-	1.89 e-02	-	1.33 e-02	-
60x60	8.23 e-07	2.10	8.26 e-03	2.04	8.26 e-03	2.04	6.06 e-03	1.98
80x80	4.00 e-07	2.50	4.02 e-03	2.50	4.02 e-03	2.50	3.07 e-03	2.36
$M = 10^{-3}$								
40x40	1.93 e-08	-	1.89 e-02	-	1.89 e-02	-	1.33 e-02	-
60x60	8.23 e-09	2.10	8.27 e-02	2.04	8.27 e-02	2.04	6.06 e-03	1.98
80x80	4.00 e-09	2.50	4.02 e-03	2.50	4.02 e-03	2.50	3.07 e-03	2.36
$M = 10^{-4}$								
40x40	2.43 e-10	-	1.89 e-02	-	1.89 e-02	-	1.33 e-02	-
60x60	1.53 e-10	1.14	8.26 e-02	2.04	8.26 e-02	2.04	6.06 e-02	1.93
80x80	1.10 e-10	1.14	4.02 e-03	2.50	4.02 e-03	2.50	3.07 e-02	2.36

Also we give again the CPU times for the numerical schemes where again the algorithm is run on a single CPU of the type Intel(R) Core(TM) i5-4690 CPU with 3.50GHz on a 64-bit 4.4.176-96 linux system, see 4.3.

TABLE 4.3. CPU times in seconds for the smooth Gresho vortex on different resolutions and different Mach numbers.

Resolution	Mach number		
	10^{-2}	10^{-3}	10^{-4}
40x40	115	115	115
60x60	519	520	519
80x80	1392	1397	1397

Again we see that on all resolutions the CPU times for the scheme S_M are stable under variation of the Mach number.

4.4. Kelvin Helmholtz Instability

The last test case concerns the approximation of a Kelvin-Helmholtz instability. The idea is to introduce a non steady flow problem to further investigate the influence of the numerical diffusion on the quality of the numerical approximations. The setup is also taken from [26], where the shear instability is triggered artificially to enforce a specific behavior of the resulting vortexes. This gives the possibility to compare the results for different schemes. Therefore the initial conditions are set as

$$\rho = \begin{cases} \rho_1 - \rho_m \exp\left(\frac{y-0.25}{L}\right) & \text{if } 0 \leq y \leq 0.25, \\ \rho_2 + \rho_m \exp\left(\frac{-y+0.25}{L}\right) & \text{if } 0.25 \leq y \leq 0.5, \\ \rho_2 + \rho_m \exp\left(\frac{y-0.75}{L}\right) & \text{if } 0.5 \leq y \leq 0.75, \\ \rho_1 - \rho_m \exp\left(\frac{-y+0.75}{L}\right) & \text{if } 0.75 \leq y \leq 1, \end{cases}$$

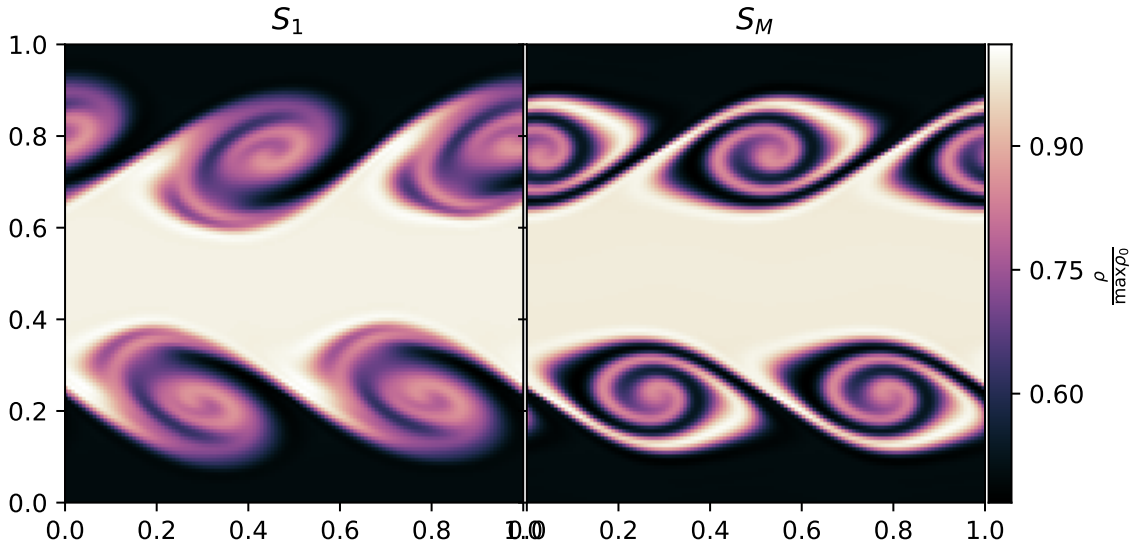


FIGURE 4.4. Kelvin-Helmholtz Instability computed with the schemes S_1 and S_M on a 128×128 grid.

and

$$u = \begin{cases} u_1 - u_m \exp\left(\frac{y-0.25}{L}\right) & \text{if } 0 \leq y \leq 0.25, \\ u_2 + u_m \exp\left(\frac{-y+0.25}{L}\right) & \text{if } 0.25 \leq y \leq 0.5, \\ u_2 + u_m \exp\left(\frac{y-0.75}{L}\right) & \text{if } 0.5 \leq y \leq 0.75, \\ u_1 - u_m \exp\left(\frac{-y+0.75}{L}\right) & \text{if } 0.75 \leq y \leq 1, \end{cases}$$

and $p = 2.5$. The parameters are

$$\begin{aligned} \rho_1 &= 1.0 & \rho_2 &= 2.0 & \rho_m &= \frac{\rho_1 - \rho_2}{2}, \\ u_1 &= 1.0 & u_2 &= 2.0 & u_m &= \frac{u_1 - u_2}{2}, \end{aligned}$$

and $L = 0.025$. The computational domain is $D = [0, 1] \times [0, 1]$ and periodic boundary conditions are imposed. The instability is triggered by a perturbation in the vertical velocity as

$$v = 10^{-2} \sin(2\pi x)$$

and the simulations are performed with a Mach number of $M = 10^{-2}$. The results are depicted in Figure 4.4 and Figure 4.5.

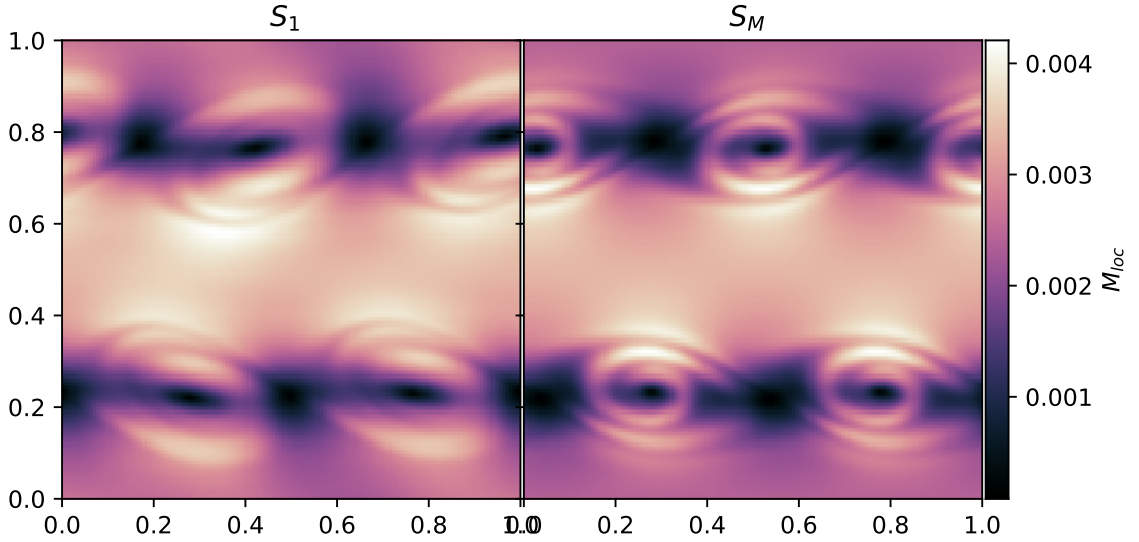


FIGURE 4.5. Kelvin-Helmholtz Instability computed with the schemes S_1 and S_M on a 128×128 grid.

From Figure 4.5 we have that the flow regime is in the regime of a Mach number $M \approx 10^{-4}$. From the Gresho vortex test we therefore expect a significant improvement by the introduction of the new relaxation scheme S_M . The superior performance can be seen in Figure 4.4. The resulting vortices are better resolved by the scheme S_M than with the scheme S_1 .

As in the Gresho vortex test case we now also investigate the evolution of the total kinetic energy, given in Figure 4.6. As can be seen from this picture, the scheme S_1 has strong problems with the convergence. In contrast to the scheme S_M where the evolution of the total kinetic energy is stable.

5. Conclusion

In this work we are concerned with the low Mach number approximation of flows governed by the compressible Euler equations. We have used the standard Suliciu relaxation technique and showed, that it is not useful for the approximation of these flow regimes. Then we construct a modified relaxation scheme and show, that the numerical diffusion of the upwind scheme is controlled in the low Mach number case, that the relaxation scheme is robust with respect to the positivity of density and internal energy and show the asymptotic preserving property of the new scheme. We then give numerical tests to show the superior performance of the modified relaxation scheme compared to a standard scheme.

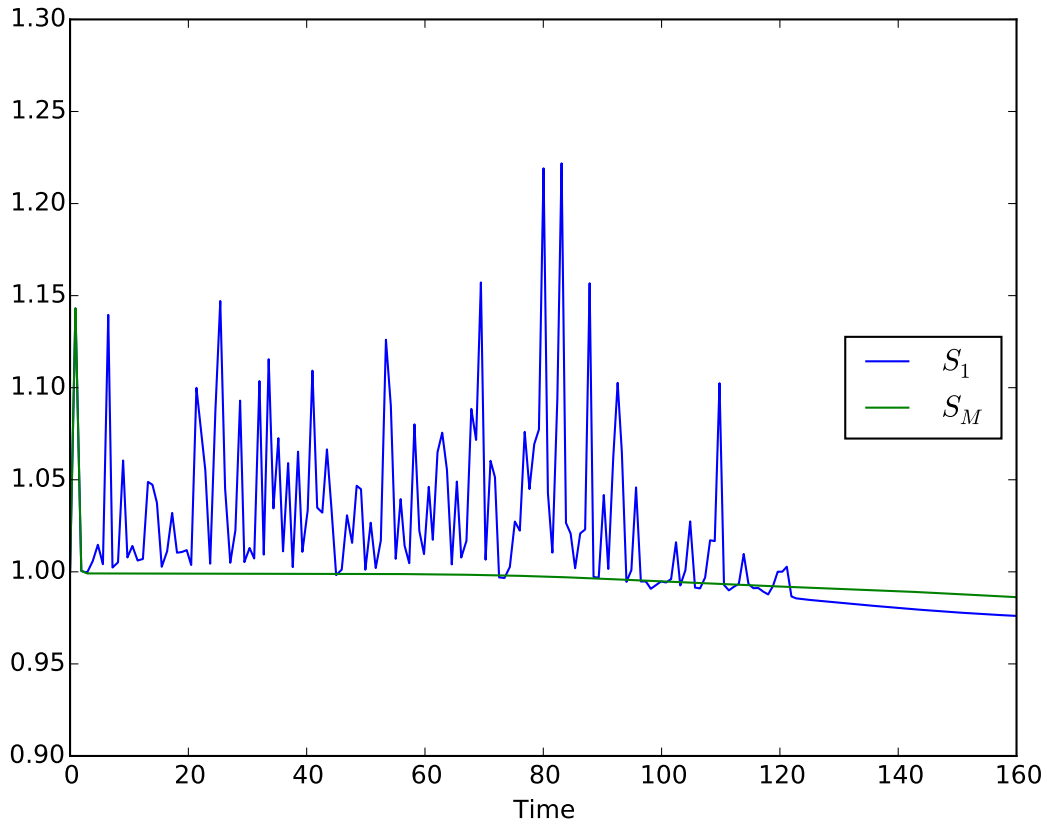


FIGURE 4.6. Kelvin-Helmholtz Instability: Evolution of the normed total kinetic energy for the schemes S_1 and S_M on a 128×128 grid.

References

- [1] W. Barsukow, P. Edelmann, C. Klingenberg, F. Miczek, and F. Röpke. A numerical scheme for the compressible low-Mach number regime of idela fluid dynamics. *J. Sci. Comput.*, 72(2):623–646, 2017.
- [2] M. Baudin, C. Berthon, F. Coquel, R. Masson, and Q. H. Tran. A relaxation method for two-phase flow models with hydrodynamic closure law. *Numer. Math.*, 99(3):411–440, 2005.
- [3] G. Bispen, K. R. Arun, M. Lukáčová-Medvidóvá, and S. Noelle. IMEX large time step finite volume methods for low Froude number shallow water flows. *Commun. Comput. Phys.*, 16(2):307–347, 2014.
- [4] S. Boscarino, L. Pareschi, and G. Russo. Implicit-Explicit Runge–Kutta Schemes for Hyperbolic Systems and Kinetic Equations in the Diffusion Limit. *SIAM J. Sci. Comput.*, 35, 2013.
- [5] F. Bouchut. *Nonlinear Stability of Finite Volume Methods for Hyperbolic Conservation Laws and Well-Balanced Schemes for Sources*. Birkhäuser, 2004.
- [6] C. Chalons, F. Coquel, E. Godlewski, P.-A. Raviart, and N. Seguin. Godunov-type schemes for hyperbolic systems with parameter-dependent source. The case of Euler system with friction. *Math. Models Methods Appl. Sci.*, 20(11):2109–2166, 2010.

- [7] G. Q. Chen, C. D. Levermore, and T.-P. Liu. Hyperbolic conservation laws with stiff relaxation terms and entropy. *Commun. Pure Appl. Math.*, 47:787–830, 1994.
- [8] F. Coquel and B. Perthame. Relaxation of Energy and Approximate Riemann Solvers for General Pressure Laws in Fluid Dynamics. *SIAM J. Numer. Anal.*, 35(6):2223–2249, 1998.
- [9] A. De Coninck, B. De Baets, D. Kourounis, F. Verbosio, O. Schenk, S. n Maenhout, and J. Fostier. Needles: Toward Large-Scale Genomic Prediction with Marker-by-Environment Interaction. *Genetics*, 203(1):543–555, 2016.
- [10] P. Degond and M. Tang. All Speed Scheme for the Low Mach Number Limit of the Isentropic Euler Equations. *Commun. Comput. Phys.*, 10(1):1–31, 2011.
- [11] S. Dellacherie. Analysis of Godunov type schemes applied to the compressible Euler system at low Mach number. *J. Comput. Phys.*, 229(4):978–1016, 2010.
- [12] G. Dimarco and L. Pareschi. Asymptotic Preserving Implicit-Explicit Runge–Kutta Methods for Nonlinear Kinetic Equations. *SIAM J. Numer. Anal.*, 51, 2013.
- [13] E. Feireisl, C. Klingenberg, and S. Markfelder. On the low Mach number limit for the compressible Euler system. preprint, <https://arxiv.org/abs/1804.09509>.
- [14] E. Godlewski and P.-A. Raviart. *Numerical approximation of hyperbolic systems of conservation laws*, volume 118 of *Applied Mathematical Sciences*. Springer, 1996.
- [15] H. Guillard and A. Murrone. On the behavior of upwind schemes in the low Mach number limit: II. Godunov type schemes. *Computers & Fluids*, 33:655–675, 2004.
- [16] H. Guillard and C. Viozat. On the behaviour of upwind schemes in the low Mach number limit. *Computers & Fluids*, 28:63–86, 1999.
- [17] J. Haack, S. Jin, and J. Liu. An all-speed asymptotic-preserving method for the isentropic Euler and Navier-Stokes equations. *Commun. Comput. Phys.*, 12(4):955–980, 2012.
- [18] A. Harten, P. D. Lax, and B. Van Leer. On upstream differencing and Godunov-type schemes for hyperbolic conservation laws. *SIAM Rev.*, 25:35–61, 1983.
- [19] S. Jin. Efficient Asymptotic-Preserving (AP) Schemes For Some Multiscale Kinetic Equations. *SIAM J. Sci. Comput.*, 21(2):441–454, 1999.
- [20] C. A. Kennedy and M. H. Carpenter. Additive Runge-Kutta Schemes for Convection-Diffusion-Reaction Equation. Technical report, NASA Technical Memorandum, 2001.
- [21] S. Klainerman and A. Majda. Singular limits of quasilinear hyperbolic systems with large parameters and the incompressible limit of compressible fluids. *Commun. Pure Appl. Math.*, 34(4):481–524, 1981.
- [22] R. Klein. Semi-implicit extension of a godunov-type scheme based on low mach number asymptotics I: One-dimensional flow. *J. Comput. Phys.*, 121(2):213–237, 1995.
- [23] R. Klein, N. Botta, T. Schneider, C. D. Munz, S. Roller, A. Meister, L. Hoffmann, and T. Sonar. Asymptotic adaptive methods for multi-scale problems in fluid mechanics. *J. Eng. Math.*, 39(1):261–343, 2001.
- [24] D. Kourounis, A. Fuchs, and O. Schenk. Towards the Next Generation of Multiperiod Optimal Power Flow Solvers. *IEEE Trans. Power Syst.*, 33(4):4005–4014, 2018.
- [25] F. Miczek. *Simulation of low Mach number astrophysical flows*. PhD thesis, München, Technische Universität München, Diss., 2013.
- [26] F. Miczek, F. Röpke, and P. Edelmann. A new numerical solver for flows at various Mach numbers. *Astron. Astrophys.*, 576(A50):16, 2015.
- [27] S. Noelle, G. Bispen, K. R. Arun, M. Lukáčová-Medvidóvá, and C. D. Munz. An Asymptotic Preserving all Mach Number Scheme for the Euler Equations of Gas Dynamics. *SIAM J. Sci. Comput.*, 36(6):989–1024, 2014.

- [28] B. Perthame and C. W. Shu. On positivity preserving finite volume schemes for Euler equations. *Numer. Math.*, 73(1):119–130, 1996.
- [29] P. L. Roe. Approximate Riemann solvers, parameter vectors, and difference schemes. *J. Comput. Phys.*, 43(2):357–372, 1981.
- [30] G. A. Sod. A survey of several finite difference methods for systems of nonlinear hyperbolic conservation laws. *J. Comput. Phys.*, 27(1):1–31, 1978.
- [31] I. Suliciu. On modelling phase transitions by means of rate-type constitutive equations, shock wave structure. *Int. J. Eng. Sci.*, 28:829–841, 1990.
- [32] I. Suliciu. Some stability-instability problems in phase transitions modelled by piecewise linear elastic or viscoelastic constitutive equations. *Int. J. Eng. Sci.*, 30:483–494, 1992.
- [33] E. Turkel. Preconditioned Methods for Solving the Incompressible and Low Speed Compressible Equations. *J. Comput. Phys.*, 72, 1987.
- [34] F. Verbosio, A. De Coninck, D. Kourounis, and O. Schenk. Enhancing the scalability of selected inversion factorization algorithms in genomic prediction. *J. Comput. Sci.*, 22(Supplement C):99–108, 2017.
- [35] J. M. Weiss and W. A. Smith. Preconditioning applied to variable and constant density flows. *AIAA J.*, 33(11):2050–2057, 1995.
- [36] G. B. Whitham. *Linear and nonlinear waves*. Pure and Applied Mathematics. John Wiley & Sons, 1974.